Received: 16 January 2020 | Revised: 7 April 2020 | Accepted: 15 April 2020

DOI: 10.1002/wcms.1480

Check for updates

WIREs COMPUTATIONAL MOLECULAR SCIENCE WILEY

ADVANCED REVIEW

Decoding chemical information from vibrational spectroscopy data: Local vibrational mode theory

Elfi Kraka[1] | **Wenli Zou**[2] | **Yunwen Tao**[1]

[1]Department of Chemistry, Southern Methodist University, Dallas, Texas

[2]Institute of Modern Physics, Northwest University and Shaanxi Key Laboratory for Theoretical Physics Frontiers, Xi'an, Shaanxi, PR China

Correspondence
Elfi Kraka, Department of Chemistry, Southern Methodist University, 3215 Daniel Avenue, Dallas, TX 75275-0314.
Email: ekraka@gmail.com

Funding information
National Natural Science Foundation of China, Grant/Award Number: 21673175; National Science foundation, NSF, Grant/Award Number: CHE 1464906

Abstract

Modern vibrational spectroscopy is more than just an analytical tool. Information about the electronic structure of a molecule, the strength of its bonds, and its conformational flexibility is encoded in the normal vibrational modes. On the other hand, normal vibrational modes are generally delocalized, which hinders the direct access to this information, attainable only via local vibration modes and associated local properties. Konkoli and Cremer provided an ingenious solution to this problem by deriving local vibrational modes from the fundamental normal modes, obtained in the harmonic approximation of the potential, via mass-decoupled Euler–Lagrange equations. This review gives a general introduction into the local vibrational mode theory of Konkoli and Cremer, elucidating how this theory unifies earlier attempts to obtain easy to interpret chemical information from vibrational spectroscopy: (a) the local mode theory furnishes bond strength descriptors derived from force constant matrices with a physical basis, (b) provides the highly sought after extension of the Badger rule to polyatomic molecules, (c) and offers a simpler way to derive localized vibrations compared to the complex route via overtone spectroscopy. Successful applications are presented, including a new measure of bond strength, a new detailed analysis of infrared/Raman spectra, and the recent extension to periodic systems, opening a new avenue for the characterization of bonding in crystals. At the end of this review the LMODEA software is introduced, which performs the local mode analysis (with minimal computational costs) after a harmonic vibrational frequency calculation optionally using measured frequencies as additional input.

This article is categorized under:

Structure and Mechanism > Molecular Structures

Theoretical and Physical Chemistry > Spectroscopy

Software > Quantum Chemistry

Electronic Structure Theory > Ab Initio Electronic Structure Methods

KEYWORDS

bonding in solid state, decomposition of IR/Raman spectra, LMODEA, local mode analysis, local mode force constants, vibrational spectroscopy

 © 2020 Wiley Periodicals LLC.

1 | INTRODUCTION

Over the past decades, vibrational spectroscopy has developed into an important analytical tool[1–21] with ample applications in chemistry and beyond.[22–31] Today modern vibrational spectroscopy has much more to offer; detailed information on the electronic structure of a molecule and its chemical bonds is encoded in the normal vibrational modes, ready to be deciphered. With the increasing number of available high precision measured spectra, complemented with theoretical calculations, vibrational spectroscopy can become an excellent source for decoding electronic structure information of a molecule; in particular providing a new quantitative measure of the intrinsic strength of a chemical bond.

As revealed in Figure 1, the idea of characterizing a chemical bond via the stretching force constant dates back to the 1920s and 1930s. In 1934, Badger published an inverse power relationship between the bond length and the stretching force constant for a series of diatomic molecules, termed the so-called *Badger rule*.[33] While this rule works fine for diatomic molecules, its extension to polyatomic molecules turned out to be difficult because normal vibrational modes tend to delocalize over the molecule rather than being localized in a specific bond; where this mode localization is a prerequisite for using the stretching force constant as a suitable bond strength measure.[34,35] As shown in Figure 1, the following decades saw various efforts to overcome this problem via modification and extension of the original Badger rule. In many cases these extensions only worked for specific sets of molecules;[32] and more importantly, the simplicity of Badger's original idea diminished. Therefore, it became clear that a successful generalization of the Badger rule to polyatomic molecules required the solution to the basic problem, namely to revert to local stretching force constants derived from local vibrational modes.

Before a more detailed discussion of the local vibrational mode theory of Konkoli and Cremer,[36–40] which led to the generalized Badger rule[32] and a new measure of the intrinsic strength of a chemical bond, is provided, some remarks on the origin of the term *local modes* are necessary (see summary in Figure 2).

In 1929, Ellis[41] introduced a local X-H Morse oscillator description to explain overtone absorptions in hexane, cyclohexane, benzene, chloroform, and aniline. The anharmonic bond oscillators became decoupled with increasing stretching energies, leading to a local description and the original idea of *local modes*. This local mode concept enabled a refined way of describing highly excited stretching states of anharmonic vibrations. But it was in contrast to the normal-mode-based vibrational picture where all atoms of the molecule move in phase during a normal vibration. In the following two decades, Mecke and co-workers[42–46] explored the anharmonic decoupling of the local modes and their relation to normal mode theory, and they advocated the use of local modes instead of normal modes. However, with overtone spectroscopy at its infancy and difficulties formulating exact vibrational Hamiltonians that include all vibrational degrees of freedom and not only the stretching vibrations, the simpler normal mode description based on a harmonic potential remained favored. In 1940, Darling and Dennison found evidence for a new and important

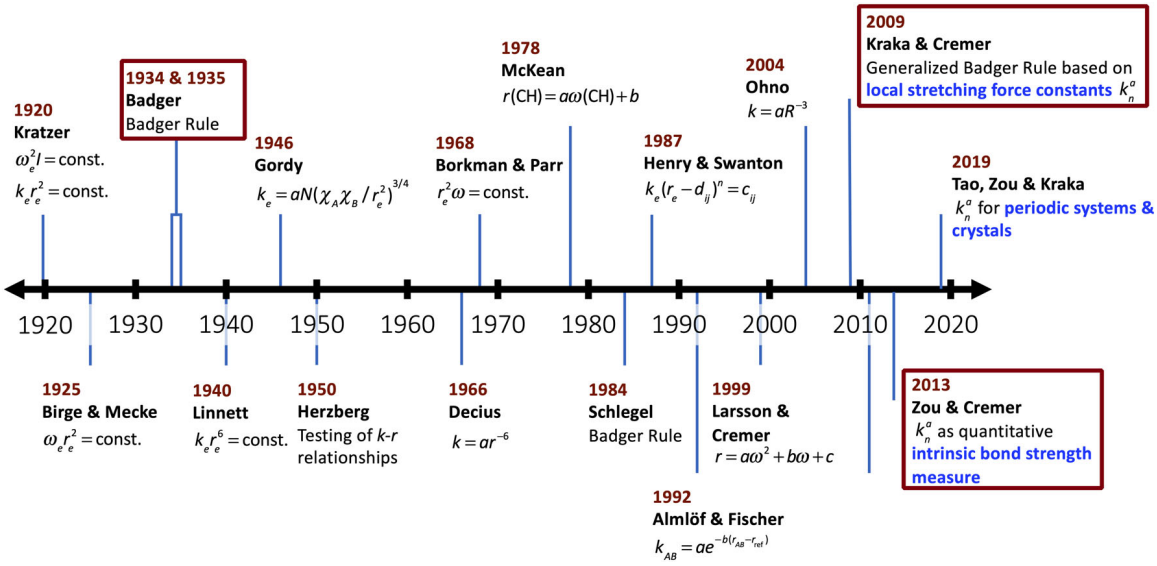

FIGURE 1 Use of stretching force constants and frequencies as bond strength descriptors based on the Badger rule. A comprehensive overview is given in Table 4.1 of Reference 32

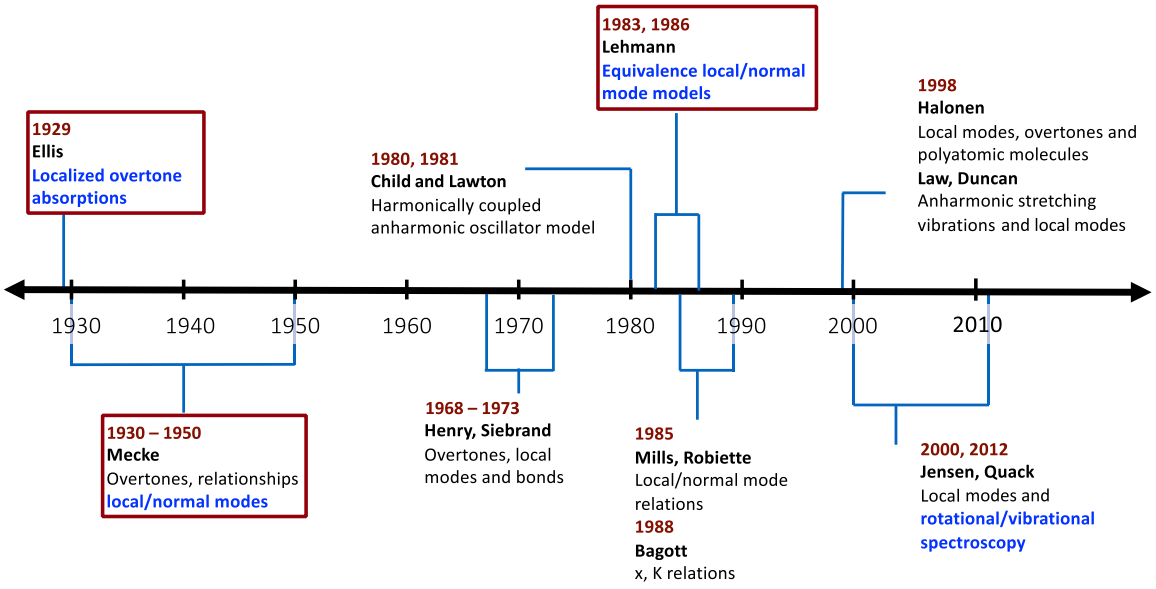

FIGURE 2 Local modes and overtone spectroscopy

resonance between the overtone levels of the normal mode symmetric and antisymmetric stretching vibrations in water, later known as Darling–Dennison resonance.[47] Since they could explain this resonance within the context of normal modes, this also added to the popularity of normal modes. Therefore, it took until the late 1960s for the local mode models to be rediscovered; primarily through the work of Henry, Siebrand, and others[48–54] who established the generality of local mode behavior in overtone spectra for a wide variety of molecules. In addition, Child and Lawton derived local and normal vibrational states with a harmonically coupled anharmonic-oscillator model.[55–58] This work was followed by important contributions of Lehmann,[59,60] and Mills and Robiette,[61] on the relationship of local and normal mode models; Bagott,[62] who interrelated normal and local mode descriptions with the so-called *x*, *K* relations combining normal mode anharmonicity constants *x* and the Darling–Dennison resonance constants *K*; which was further developed by Law and Duncan[63–65] via their anharmonically-coupled local mode to normal mode Hamiltonian transformations. A more comprehensive overview of this important time period has been given in several reviews, for example, by Quack,[66] Halonen,[67] and Jensen.[68] In the last 20 years it has been theoretically predicted and to a large extent experimentally verified, that local mode behavior is not only induced by vibrational excitation, but also by excitation of rotational motion.[68–70]

Near-infrared spectroscopy (NIRS) has substantially developed over the last few decades as an invaluable and rich source of information on the anharmonic nature of molecular vibrations.[9] It has entered modern analytical applications, even moving in the direction of complex systems and biomolecules.[71] However, the intrinsic complexity of NIR spectra compared to conventional mid-range infrared (MIR) spectra focusing on fundamental vibrations, forces the extensive use of pretreatment methods and causes challenges for the data analysis.[9] Also, the emerging field of theoretical NIRS is faced with several challenges. While the calculation of MIR or Raman spectra in the harmonic approximation is nowadays routine, NIR modes require to go beyond the harmonic approximation. Accurate variational methods are practically applicable to the simplest systems only. More practical methods are for example vibrational self-consistent field (VSCF) methods.[72–74] The key economical feature of these methods is the approximate treatment of inter-modal anharmonicity; like in Hartree Fock theory any given mode feels an averaged effect resulting from all other modes. Another class of anharmonic methods is based on perturbation theory of the molecular Hamiltonian after its expansion via power series of products of vibrational and rotational operators, also referred to as vibrational perturbation theory.[75] This approach is particularly appealing for its computational efficiency in treating medium-to-large systems,[75] and has been extended to simulations of IR absorptions for molecular systems in excited electronic states.[76] Recently, the use of molecular dynamics (MD) simulations have been advocated.[77] Although anharmonic simulations of vibrational spectra of larger molecules including transition metal complexes[78,79] and/or biomolecules are now in reach,[80,81] it is still unclear how one could derive generally applicable bond strength measures from these local modes, and the search for other alternatives related to vibrational spectroscopy has continued over the past decades, as is summarized in Figure 3.

In 1939 Wilson[82] and in 1940 El'yashevich[83] independently derived the secular equation for molecular vibrations in matrix from, frequently referred to as the *Wilson GF method*. Central to their work was the extension from Cartesian coordinates **x** to internal coordinates **q** via the so-called **B** matrix (details are given below). It was recognized that expressing the potential energy of a vibrating molecule in terms of internal coordinates **q**, such as interatomic distances, bond angles, dihedral angles, and so on led to an easier physical interpretation; and that the force constants derived from these potentials, appeared to carry over from one similar molecule to another. This important observation, combined with earlier work on vibrational spectra and molecular structure, formed the basis for the development of the force field methods. In this connection, the pioneering studies of Andrews[84] on the relation between Raman spectra and structure of small organic molecules, and Dennison's[85,86] work on infrared spectra of polyatomic molecules have to be mentioned, as well as the extensive work of Linnett.[87,88] Andrews's promising assumption that "the restoring forces in vibrating molecules consist in first approximation of harmonic forces along the directions of the chemical bonds and perpendicular to them"[84] was realized in one of the first empirical molecular mechanics force fields, for example, the Urey–Bradley force field.[89] The transition from the original idea of using force fields to reproduce or predict vibrational spectra to the application of force fields for the study of molecular structure started in the 1940s with Hill's work on steric effects,[90] the studies of Dostrovsky et al. on S_N2 reactions,[91] Gordy's early work on force constants and molecular properties,[92] as well as the work of Westheimer, leading to one of the first force fields for organic molecules.[93,94] A detailed overview of the subsequent development of the field of molecular mechanics and force field calculations would be beyond the scope of this article, therefore we refer the reader to the work of Allinger[95,96] or Machida[97] for examples.

The original work on force fields (i.e., finding the optimal force constant values to match experimental spectra) triggered the idea of using bond stretching force constants, contained in the force constant matrix $\mathbf{F}^q$, that is, the Hessian in internal coordinates, as a bond strength measure. However, it was soon realized that $\mathbf{F}^q$ depends on the choice of internal coordinates used to describe the molecular geometry, thus leading to force constants values which depend on the definition of all other internal coordinates, so that their transferability is rather limited. Decius suggested to solve this problem by using the inverse of the force constant matrix,[98] because the inverse is invariant under coordinate transformations.[99] In 1963 he derived the inverse force constant matrix, which he called *compliance matrix* $\mathbf{\Gamma}$, from the potential energy of a molecule written as a quadratic form in terms of generalized displacement forces and proved that

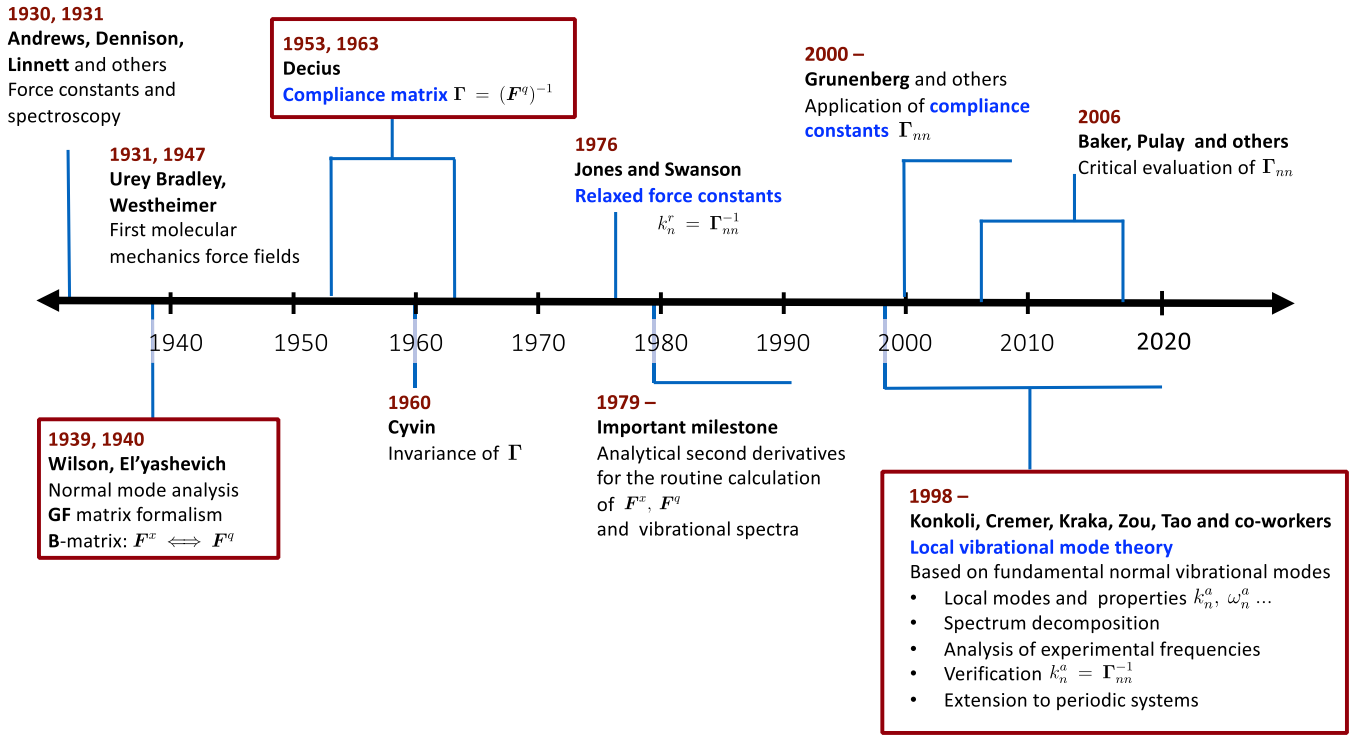

FIGURE 3 Development of bond strength descriptors based on the force constant matrix $\mathbf{F}^q$

Γ is independent of the choice of the internal coordinates.[100] Based on these findings he promoted the idea to use the diagonal elements of **Γ**, the so-called *compliance constants* Γ_{nn} as bond strength descriptors.[100] As the units of compliance constants are reciprocal force constant units, Jones and Swanson suggested to use the reciprocal compliance constants instead, which they coined *relaxed force constants*,[101] complying with general chemical thinking that a stronger bond should be assigned to a larger force constant. An important factor promoting the use of Hessian derived bond strength descriptors was the development of analytic second energy derivatives for routine ab initio calculations of force fields and vibrational spectra, moving theoretical vibrational spectroscopy to another level. In 1979 Pople and co-workers reported analytical Hessians for Hartree Fock theory and Møller Plesset perturbation theory of second order,[102] incorporating the early ideas of Gerratt and Mills.[103] The work on analytic second derivative techniques quickly stretched across the field of theoretical chemistry, as is documented in the work of Pulay,[104–106] Schaefer,[107–110] Handy,[111–113] Bartlett,[114,115] and others,[116–120] published in the 1980s, just to give a few examples. Some comprehensive overviews can be found for example in References 121–128. One can say that even today any new computational method strongly benefits from the availability of first and second analytical derivatives.

Over the past decades, the use of compliance constants and relaxed force constants as bond strength descriptors has become popular.[129–136] Some concerns were raised with regard to weak chemical interactions suggesting that in these cases the compliance constants should be complemented with an electron density and/or population analysis.[137,138] In addition, the use of the off-diagonal compliance matrix elements Γ_{ij} as *coupling constants*[131,133] to describe the coupling between compliance constants Γ_{ii} and Γ_{jj} has been questioned. Whereas the off-diagonal Hessian matrix element F_{ij}^{q} has the meaning of a coupling force constant,[34] describing the coupling between internal coordinate i and j, this is not necessarily true for Γ_{ij}, because Γ_{ij} is not the reciprocal of F_{ij}^{q}. The most serious concern however has been the lack of a physical basis and link to vibrational spectroscopy, as compliance constants originated from a mathematical recipe, as well as the lack of associated local modes, frequencies, intensities, and other properties. As is summarized in Figure 3, the local vibrational mode theory of Konkoli and Cremer[36–40] provides a physically based framework resolving these concerns and in addition to local mode force constants, has led to a repertoire of tools for the analysis of vibrational spectra being based on normal vibrational modes in the harmonic approximation; which will be discussed in the next chapter. Before doing so, it is useful to point out additional use of the term *local mode* in the literature.

1. McKean's *isolated modes* obtained for CH stretching vibrations via isotope substitution[139] can be considered as experimental counterparts of the Konkoli–Cremer local vibrational modes,[140] as will be discussed below. McKean's underlying idea was to replace all but one H atom of a hydrocarbon molecule with deuterium (i.e., investigating perdeuterated isotopomers with just one H atom in a CD_2H or CDH group). In this way he could minimize the coupling of the CH stretching mode with other modes in hydrocarbons to less than 5 cm^{-1}.[139]
2. In solid state physics, the term *local modes* is used in several ways.[141–143] In solid state Raman spectroscopy, one often speaks of external and internal crystal lattice vibrational modes, particularly for molecular crystals.[144] The external crystal lattice vibrations are considered the collective motion of the molecules in the crystal as a whole, whereas the internal crystal lattice vibrational modes, (called *local modes* in this connection) arise from the coupling of the vibrational modes of the individual molecular species. Often the vibrational mode(s) caused by an impurity in a solid material is (are) called *local modes*[145,146] and quasi-local modes are considered as vibrational states physically located next to defects in an ideal lattice.[147] Similar to the "impurity" concept, materials scientists refer to local vibrational modes as Raman peaks corresponding to the active modes of atomic implants, substitutional atoms, or dopants in thin solid films.[148–151] It has to be noted that the use of the term *local modes* in solid state physics is completely different from our use of local modes for periodic systems, which will be discussed in Section 3.
3. Reiher and co-workers[152–154] calculated unitarily transformed normal modes of a polymer associated with a given band in the vibrational spectrum, where the criteria for the transformation are inspired by those applied for the localization of molecular orbitals. Similar to Reiher's work, Cheng and Steele[155] and Panek and co-workers[156] also employed a unitary transformation to derive *localized modes* from the normal modes to be used for VSCF calculations to account for anharmonicity in simulated vibrations. The authors speak in these cases of local vibrational modes, because the modes are localized in just a few subunits of the entire system. However, these so-called *localized modes* are still delocalized within the subunits.

2 | THEORY OF LOCAL VIBRATIONAL MODES

2.1 | Lagrangian approach to vibrational spectroscopy

The Lagrangian mechanics[157] provides a convenient way to describe the atomic motions during a molecular vibration within the classical picture by solving the Euler–Lagrange equations

$$\frac{d}{dt}\frac{\partial L(\mathbf{x},\dot{\mathbf{x}})}{\partial \dot{x}_i} - \frac{\partial L(\mathbf{x},\dot{\mathbf{x}})}{\partial x_i} = 0,\ i = 1,\ldots,3N, \tag{1}$$

where the Lagragian $L(\mathbf{x},\dot{\mathbf{x}})$ is defined as the difference of the kinetic energy $T(\dot{\mathbf{x}})$ and the potential energy $V(\mathbf{x})$ of the vibrational mode.

$$L(\mathbf{x},\dot{\mathbf{x}}) = T(\dot{\mathbf{x}}) - V(\mathbf{x}), \tag{2}$$

$$= \frac{1}{2}\dot{\mathbf{x}}\dagger\mathbf{M}\dot{\mathbf{x}} - \frac{1}{2}\mathbf{x}^{\dagger}\mathbf{F}^{x}\mathbf{x}. \tag{3}$$

Vector $\mathbf{x}$ contains the $3N$ Cartesian displacement coordinates of the molecule being composed of N atoms describing the deviation of the atoms from their equilibrium position during the vibration, and a dot over a variable (e.g., $\dot{\mathbf{x}}$) denotes differentiation with respect to time. $\mathbf{F}^{x}$ is the force constant matrix (Hessian) in Cartesian coordinates $\mathbf{x}$. The diagonal mass matrix $\mathbf{M}$ contains each atomic mass three times to account for the motion in the x-, y-, and z-direction, repectively, that is, $M_{i,i} = \{m_1, m_1, m_1, m_2, m_2, m_2, \ldots\}$. Both square matrices have the dimension $(3N \times 3N)$. The potential energy $V(\mathbf{x})$ is zero when the atoms are in their equilibrium positions and greater than zero otherwise. The † superscript denotes transpose for both vectors and matrices.

The Lagrangian can be also expressed in terms of $N_{vib} = (3N - \Sigma)$ internal coordinates $\mathbf{q}$; (Σ: number of translations and rotations; 6 for nonlinear and 5 for linear molecules)[34]:

$$L(\mathbf{q},\dot{\mathbf{q}}) = T(\dot{\mathbf{q}}) - V(\mathbf{q}), \tag{4}$$

$$= \frac{1}{2}\dot{\mathbf{q}}\dagger\mathbf{G}^{-1}\dot{\mathbf{q}} - \frac{1}{2}\mathbf{q}^{\dagger}\mathbf{F}^{q}\mathbf{q}. \tag{5}$$

$\mathbf{F}^{q}$ is the force constant matrix in internal coordinates $\mathbf{q}$, $\mathbf{G}$ is the Wilson $\mathbf{G}$ matrix,[34] also called "inverse kinetic energy" matrix. $\mathbf{G}$ is symmetric about its main diagonal (i.e., $G_{ij} = G_{ji}$) and contains only real elements. Both $\mathbf{F}^{q}$ and $\mathbf{G}$ are square matrices with the dimension $N_{vib} \times N_{vib}$.

The relationship between internal and Cartesian coordinates is provided by the Wilson $\mathbf{B}$ matrix,[34] a rectangular $(N_{vib} \times 3N)$ matrix containing the first derivatives of the internal coordinates $q_n (n = 1, 2, 3 \ldots N_{vib})$ with respect to the Cartesian coordinates $x_i (i = 1, 2, 3 \ldots 3N)$,

$$\mathbf{B}_n = \frac{\delta q_n(\mathbf{x})}{\delta x_i}. \tag{6}$$

The transformation between internal and Cartesian coordinates via Equation (6) can be extended to puckering coordinates, symmetry coordinates or other special coordinates, for example, coordinates including dummy atoms as long as the first derivative of the considered coordinates with respect to Cartesian coordinates can be worked out via analytic or numerical differentiations.[34] The $\mathbf{B}$ matrix also provides the important link between the $\mathbf{M}$ and $\mathbf{G}$ matrices via the following relationship.[34,82]

$$\mathbf{G} = \mathbf{B}\mathbf{M}^{-1}\mathbf{B}^{\dagger}. \tag{7}$$

Equation (5) reveals that there are two different coupling mechanisms between the vibrational modes, *mass coupling* due to the off-diagonal elements of the Wilson $\mathbf{G}$ matrix, reflecting pairwise kinetic coupling between the internal

coordinates and *electronic coupling* due to the off-diagonal coupling force constants of the $\mathbf{F}^q$ matrix.[34] It has to be noted that in this connection the term *electronic coupling* refers to the potential energy and should not be confused with the use of the term *electronic coupling* in electron and/or excitation energy transfer theory.[158,159]

The electronic coupling can be eliminated via the Wilson GF-matrix formalism applied to Equation (1),[34,82,160,161] that is, solving the vibrational secular equation:

$$\mathbf{F}^x\mathbf{L} = \mathbf{M}\mathbf{L}\boldsymbol{\Lambda}. \tag{8}$$

Matrix $\boldsymbol{\Lambda}$ is a diagonal matrix with the eigenvalues λ_μ, which leads to the N_{vib} (harmonic) vibrational frequencies ω_μ according to $\lambda_\mu = 4\pi^2c^2\omega_\mu^2$, and $\mathbf{L}$ collects the vibrational eigenvectors $\mathbf{l}_\mu$ in its columns, with the following properties

$$\mathbf{L}^\dagger\mathbf{F}^x\mathbf{L} = \mathbf{F}^\mathbf{Q} = \mathbf{K}, \tag{9}$$

$$\mathbf{L}^\dagger\mathbf{M}\mathbf{L} = \mathbf{M}^R. \tag{10}$$

Equations (9) and (10) define the diagonal normal force constant matrix $\mathbf{F}^\mathbf{Q} = \mathbf{K}$ and the reduced mass matrix $\mathbf{M}^R$ (with elements m_μ^R), respectively. $\mathbf{Q}$ is a vector that collects the N_{vib} normal coordinates.[162] It is important to note that the diagonalization of the force constant matrix $\mathbf{F}^x$, that is, transforming to normal coordinates $\mathbf{Q}$[163–165] eliminates the off-diagonal coupling force constant matrix elements.[34] The vibrational secular equation expressed in internal coordinates $\mathbf{q}$ is given by[34]

$$\mathbf{F}^q\mathbf{D} = \mathbf{G}^{-1}\mathbf{D}\boldsymbol{\Lambda}. \tag{11}$$

$\mathbf{D}$ contains the normal mode column vectors $\mathbf{d}_\mu$ ($\mu = 1, \cdots, N_{vib}$) in internal coordinates,[34] which can be related to its counterpart $\mathbf{L}$ in Cartesian coordinates by.[164]

$$\mathbf{L} = \mathbf{C}\,\mathbf{D}, \tag{12}$$

$$\mathbf{D} = \mathbf{B}\,\mathbf{L}, \tag{13}$$

where $\mathbf{C}$ is the pseudo-inverse matrix of $\mathbf{B}$

$$\mathbf{C} = \mathbf{M}^{-1}\mathbf{B}^\dagger\mathbf{G}^{-1}, \tag{14}$$

$\mathbf{F}^q$ in Equations (5) and (11) can be calculated with the help of $\mathbf{C}$

$$\mathbf{F}^q = \mathbf{C}^\dagger\mathbf{F}^x\mathbf{C}. \tag{15}$$

2.2 | Derivation of local vibrational modes

The transformation to the diagonal force constant matrix $\mathbf{K}$ is routinely performed during a harmonic vibrational frequency calculation in standard quantum chemistry packages. However this procedure does not eliminate mass-coupling, which often has been overlooked. Konkoli and Cremer were the first to solve this problem via mass-decoupled Euler–Lagrange equations,[36–40] that is, solving the Euler Lagrange equations for a molecular fragment ϕ_n being described by an internal parameter q_n and being independent of all the other internal coordinates q_m ($m \neq n$). In their seminal paper,[36] Konkoli and Cremer derived two different ways to define the local motions of the fragment ϕ_n; Approach 1: all masses but the ones which belong to the atoms of fragment ϕ_n are zero, that is, the rest of the molecule is considered as a collection of massless points that just define the molecular geometry and Approach 2: the fragment motion is considered as a motion being obtained after relaxing all parts of the vibrating molecule but the fragment

under consideration. Because of this property, they originally coined these modes *adiabatic internal coordinate modes*.[36,37] However, over the years for reasons of simplicity, the term *local modes* was adapted.[166]

In Approach 1, the Euler–Lagrange equations (4) take the following form

$$\begin{aligned} p_n &= \frac{\delta L(\mathbf{q},\dot{\mathbf{q}})}{\delta \dot{q}_n} \neq 0, \quad \dot{p}_n = \frac{\delta V(\mathbf{q})}{\delta q_n} \neq 0, \\ p_m &= \frac{\delta L(\mathbf{q},\dot{\mathbf{q}})}{\delta \dot{q}_m} = 0, \quad \dot{p}_m = \frac{\delta V(\mathbf{q})}{\delta q_m} = 0, \quad \forall m \neq n, \end{aligned} \tag{16}$$

Equation (16) can be solved by expressing $\dot{p}_n$ as a function of a parameter λ_n leading to

$$\dot{p}_n = \frac{\delta V(\mathbf{q})}{\delta q_n} = \lambda_n \tag{17}$$

which defines a one-dimensional subspace in the full vibrational space for each internal coordinate q_n. In this way, one obtains an internal, that is, local vibration $\mathbf{a}_n$ associated with fragment ϕ_n.[36]

In Approach 2, q_n is frozen at its equilibrium value $q_n^\star$ while the other coordinates q_m $(m \neq n)$ can relax. At the minimum of the potential $V(\mathbf{q})$ then the following holds:

$$V(\mathbf{q}) = min. \tag{18}$$

$$q_n = q_n^\star. \tag{19}$$

Equations (18) and (19) can be solved using the method of Lagrange multipliers:

$$\frac{\partial}{\partial q_m}\left[V(\mathbf{q}) - \lambda_n\left(q_n - q_n^\star\right)\right] = 0 \qquad m = 1,...,N_{vib}, \tag{20}$$

leading to N_{vib} Lagrange multipliers λ_n

$$\frac{\partial V(\mathbf{q})}{\partial q_m} = \lambda_n \, \delta_{mn} \qquad m,n = 1,...,N_{vib}, \tag{21}$$

As revealed by Equations (21) and (17) Approach 1 being based on massless internal coordinates q_m $(m \neq n)$ and Approach 2 being based on the adiabatic approximation are equivalent.

After the solution of the vibrational problem in the harmonic approximation, the potential energy and each internal coordinate q_n can be expressed as functions of the N_{vib} normal coordinates Q_μ leading in this way to the determination of the n Lagrange multipliers λ_n.

$$V(\mathbf{Q}) = \frac{1}{2}\sum_{\mu=1}^{N_{vib}} k_\mu Q_\mu^2, \tag{22}$$

$$q_n(\mathbf{Q}) = \sum_{\mu=1}^{N_{vib}} D_{n\mu} Q_\mu, \tag{23}$$

$D_{n,\mu}$ is an element of the normal mode matrix $\mathbf{D}$ in the internal coordinate space and k_μ is the corresponding normal mode force constant.

Equation (22) can be solved under the constraint Equation (19)

$$\frac{\partial}{\partial Q_\mu}\left[V(\mathbf{Q})-\lambda_n\left(q_n(\mathbf{Q})-q_n^\star\right)\right]=0 \qquad \mu=1,...,N_{vib}, \tag{24}$$

leading to Equations (25) and (26)

$$\frac{\partial V(\mathbf{Q})}{\partial Q_\mu}-\frac{\partial \lambda_n}{\partial Q_\mu}\left(q_n(\mathbf{Q})-q_n^\star\right)-\lambda_n\frac{\partial\left(q_n(\mathbf{Q})-q_n^\star\right)}{\partial Q_\mu}=0, \tag{25}$$

$$\frac{\partial V(\mathbf{Q})}{\partial Q_\mu}=\lambda_n\frac{\partial q_n(\mathbf{Q})}{\partial Q_\mu}, \tag{26}$$

considering that in Equation (25) $q_n(\mathbf{Q})=q_n^\star$ at a equilibrium, that is, $\left(q_n(\mathbf{Q})-q_n^\star\right)=0$ and that $q_n^\star$ is a constant, that is, $\partial q_n^\star/\partial Q_\mu=0$.

If Equation (22) for $V(\mathbf{Q})$ and Equation (23) for $q_n(\mathbf{Q})$ are inserted into Equation (26) the result becomes

$$\frac{\partial}{\partial Q_\mu}\frac{1}{2}\sum_{\nu=1}^{N_{Vib}}k_\nu Q_\nu^2=\lambda_n\frac{\partial}{\partial Q_\mu}\sum_{\rho=1}^{N_{Vib}}D_{n\rho}Q_\rho, \tag{27}$$

which leads to

$$k_\mu Q_\mu=\lambda_n D_{n\mu}, \tag{28}$$

and for the μth normal coordinate (concerning the internal coordinate q_n) to

$$Q_\mu^{(n)}=\frac{D_{n\mu}}{k_\mu}\lambda_n, \tag{29}$$

where the superscript (n) of $Q^{(n)}$ denotes a solution obtained under the constraint for $q_n=q_n^\star$. This leads to an expression for the Lagrange multipliers λ_n in terms of $q_n^\star$

$$q_n^\star=\sum_{\mu=1}^{N_{Vib}}D_{n\mu}Q_\mu^{(n)}=\sum_{\mu=1}^{N_{Vib}}\frac{D_{n\mu}^2}{k_\mu}\lambda_n \tag{30}$$

$$\lambda_n=\frac{1}{\sum_{\mu=1}^{N_{Vib}}\frac{D_{n\mu}}{k_\mu}}q_n^\star. \tag{31}$$

Inserting Equation (31) into Equation (29) one obtains the normal coordinate $Q_\mu{}^{(n)}$ as a function of $q_n^\star$

$$Q_\mu^{(n)}=\frac{\frac{D_{n\mu}}{k_\mu}}{\sum_{\nu=1}^{N_{Vib}}\frac{D_{n\nu}^2}{k_\nu}}q_n^\star=Q_{\mu,n}^0\,q_n^\star, \tag{32}$$

with the constant $Q_{\mu,n}^0$ defining the μth component of the adiabatic vector in the normal coordinates

$$\mathbf{a}_n=\left(Q_{1,n}^0,Q_{1,n}^0,...,Q_{\mu,n}^0,...\right)^\dagger=\frac{\mathbf{K}^{-1}\mathbf{d}_n^\dagger}{\mathbf{d}_n\mathbf{K}^{-1}\mathbf{d}_n^\dagger}, \tag{33}$$

where $\mathbf{d}_n$ is the nth row of the $\mathbf{D}$ matrix, which is computed by

$$\mathbf{d}_n = \mathbf{B}_n \mathbf{L}\,, \tag{34}$$

where $\mathbf{B}_n$ is Wilson's $\mathbf{B}$ matrix34 of the n-th internal coordinate. Equation (33), which completely specifies the form of the adiabatic mode, implies the important result that what is needed for the local mode analysis are the normal mode force constant matrix $\mathbf{K}$ and the normal mode vectors $\mathbf{d}_n$ in internal coordinates, that is, the analysis can be routinely performed after a standard vibrational frequency calculation via the Wilson GF formalism.

The local mode vector $\mathbf{a}_n$ can be easily transformed into Cartesian coordinate space

$$\mathbf{a}_n^x = \mathbf{L}\mathbf{a}_n, \tag{35}$$

where $\mathbf{L}$ is the normal mode matrix in Cartesian coordinates.

2.2.1 | Properties of local modes

Once the local mode vector $\mathbf{a}_n$, which determines the movement of the molecule under the influence of parameter $q_n^\star$ is known one can define molecular properties corresponding to this motion, such as local mode force constant, local mass, and local frequency.

When the kinetic energy adopts a minimum,

$$T\left(\dot{\mathbf{x}}\right) = \frac{1}{2}\dot{\mathbf{x}}\,\dagger\mathbf{M}\,\dot{\mathbf{x}} = min, \tag{36}$$

$$\dot{q}_n = \dot{q}_n^\star = \mathbf{B}_n\,\dot{\mathbf{x}} \tag{37}$$

Equations (36) and (37) can be solved as defined in Equation (6) from

$$\frac{\partial}{\partial\,\dot{\mathbf{x}}}\left[\frac{1}{2}\dot{\mathbf{x}}\,\dagger\mathbf{M}\,\dot{\mathbf{x}} - \lambda\left(\mathbf{B}_n\,\dot{\mathbf{x}} - \dot{q}_n^\star\right)\right] = 0 \tag{38}$$

and

$$\dot{\mathbf{x}} = \mathbf{M}^{-1}\mathbf{B}_n^\dagger\lambda = \mathbf{M}^{-1}\mathbf{B}_n^\dagger\frac{\mathbf{B}_n\,\dot{\mathbf{x}}}{\mathbf{B}_n\mathbf{M}^{-1}\mathbf{B}_n^\dagger} = \frac{\mathbf{M}^{-1}\mathbf{B}_n^\dagger}{\mathbf{B_n}\mathbf{M}^{-1}\mathbf{B}_n^\dagger}\dot{q}_n^\star \tag{39}$$

Using Equation (39), Equation (36) can be rewritten as

$$T\left(\dot{q}_n^\star\right) = \frac{1}{2\mathbf{B}_n\mathbf{M}^{-1}\mathbf{B}_n^\dagger}\left(\dot{q}_n^\star\right)^2 \tag{40}$$

From Equation (40), the adiabatic mass associated with the internal coordinate q_n can be derived

$$m_n^a = \frac{1}{\mathbf{B}_n\mathbf{M}^{-1}\mathbf{B}_n^\dagger} = \frac{1}{G_{nn}} \tag{41}$$

where G_{nn} is a diagonal element of Wilson's $\mathbf{G}$ matrix[34] and superscript a denotes adiabatically relaxed, that is, derived from a local mode.

Using Equations (22), (23), (30) and (33) the potential energy in internal coordinates $\mathbf{q}$ can be rewritten

$$V(\mathbf{q}) = \frac{1}{2}\sum_{n=1}^{N_{vib}}\sum_{\mu=1}^{N_{vib}}\left[Q^0_{\mu,n}\mathbf{K}_{\mu\mu}Q^0_{\mu,n}\right]q_n^{\star 2} = \frac{1}{2}\sum_{n=1}^{N_{vib}}\left(\mathbf{a}_n^{\dagger}\mathbf{K}\mathbf{a}_n\right)q_n^{\star 2}, \tag{42}$$

defining the adiabatic, that is, local force constant as

$$k_n^a = \mathbf{a}_n^{\dagger}\mathbf{K}\mathbf{a}_n = \left(\mathbf{d}_n\mathbf{K}^{-1}\mathbf{d}_n^{\dagger}\right)^{-1}. \tag{43}$$

Local mode force constants are sensitive to differences in the electronic structure (e.g., caused by changing a substituent); because they are independent of the atomic masses they capture the pure electronic effects. In their landmark paper, Zou and Cremer[167] provided the important proof that the local stretching force constant k_n^a (AB) reflects the intrinsic strength of the bond/interaction between two atoms A and B being described by an internal coordinate q_n. They showed that k_n^a (AB) is related to the second derivative of the molecular energy with respect to q_n, that is, to the curvature of the Born-Oppenheimer potential energy surface (PES) given in a specific direction defined by q_n. They illustrated that by approximating the PES in this direction with a Morse potential and keeping the electron density frozen during the dissociation process, the intrinsic bond strength is directly related to k_n^a (AB); therefore it is justified to consider the latter as a unique and universal measure of the intrinsic strength of a chemical bond based on vibrational spectroscopy.

For the comparison of larger sets of k_n^a values, the use of a relative bond strength order (BSO n) is more convenient. Both are connected according to the generalized Badger rule derived by Cremer et al.,[32,168] via the following power relationship:

$$BSO\,n = a\left(k_n^a\right)^b. \tag{44}$$

The constants a and b are calculated from k^a values of two reference compounds with known BSO n values n_1 and n_2 via:

$$a = n_2/\left(k_2^a\right)^b, \tag{45}$$

and

$$b = ln(n_2/n_1)/ln\left(k_2^a/k_1^a\right), \tag{46}$$

and the requirement that for a force constant value of zero the corresponding BSO n value is zero. For example, for CC bonds suitable references are ethane and ethylene with bond orders $n_1 = 1$ and $n_2 = 2$, respectively.[169] In the case of more complex bonding situations such as metal–ligand bonding, guidance by Mayer bond orders[170–172] can be utilized, as discussed below.

Contrary to normal mode force constants derived from $\mathbf{F}^q$, local mode force constants are independent of the choice of the coordinates used to describe the molecule in question,[32,166,173] which provides a direct link to the compliance constants of Decius.[100] Utilizing Equation (11) the inverse force constant matrix $(\mathbf{F}^q)^{-1}$, that is, the compliance matrix $\mathbf{\Gamma}$ and its diagonal elements $\Gamma_{n,n}$ are given by

$$\mathbf{\Gamma} = \left(\mathbf{F}^q\right)^{-1} = \mathbf{D}\,\mathbf{K}\,\mathbf{D}^{\dagger}, \tag{47}$$

and

$$\left(\mathbf{\Gamma}\right)_{n,n} = \mathbf{d}_n\mathbf{K}^{-1}\mathbf{d}_n^{\dagger}, \tag{48}$$

which implies that the relaxed force constants,[101] that is, the reciprocal compliance constants[100] are identical with the local mode force constants.[166]

Using Equations (41) and (43), the adiabatic frequency can be calculated

$$\left(\omega_n^a\right)^2 = 1/\left(4\pi^2 c^2\right) \frac{k_n^a}{m_n^a} = 1/\left(4\pi^2 c^2\right) G_{nn} \mathbf{a}_n^\dagger \mathbf{K} \mathbf{a}_n. \tag{49}$$

It is important to note that local vibrational frequencies and corresponding force constants can also be derived from measured fundamental normal mode frequencies, which do not depend on any model chemistry used for the calculation, and even more importantly, which include anharmonicity effects not being captured by calculated harmonic frequencies.[174,175] The underlying assumption is that calculated normal mode vectors $\mathbf{d_\mu}$ are a reasonable approximation to the true normal mode vectors $\mathbf{d_\mu}'$. This assumption forms the basis for all frequency scaling procedures,[176–179] and therefore is well-founded. With $\mathbf{D}' \approx \mathbf{D}$ the true force constant matrix $\mathbf{F}^{q'}$ can be expressed via a perturbation added to the calculated $\mathbf{F}^q$ matrix, that is, $\mathbf{F}^{q'} = \mathbf{F}^q + \Delta\mathbf{F}^q$, as shown by Konkoli and Cremer,[40] transforming Equation (11) into

$$\left(\mathbf{F}^q + \Delta\mathbf{F}^q\right)\mathbf{D} = \mathbf{G}^{-1}\mathbf{D}(\mathbf{\Lambda} + \Delta\mathbf{\Lambda}) \tag{50}$$

The perturbation matrix $\Delta\mathbf{F}^q$ can be obtained from

$$\Delta\mathbf{F}^q\,\mathbf{D} = \mathbf{G}^{-1}\Delta\mathbf{\Lambda} \tag{51}$$

where $\Delta\mathbf{\Lambda}$ in Equations (50) and (51) collects the differences between experimental and calculated normal mode frequencies. Solving Equation (11) for $\mathbf{F}^{q'}$ leads to the true diagonal force constant matrix $\mathbf{K}'$ within the harmonic framework provided by the normal mode vectors $\mathbf{d_\mu}$. The adiabatic mode analysis can then be performed in the same way as it is for the calculated frequencies. An example can be found in Reference 174 for the water dimer.

2.2.2 | Adiabatic connection scheme

An important milestone for the local mode theory was the proof that there exists a 1:1 relationship between a complete set of nonredundant local modes and the normal modes via an adiabatic connection scheme (ACS), allowing a smooth transition from local to normal modes.[166] With the help of the compliance matrix $\mathbf{\Gamma} = (\mathbf{F^q})^{-1}$, the vibrational eigenvalue Equation (11) can be expressed as:

$$\mathbf{\Gamma}^{-1}\mathbf{D} = \mathbf{G}^{-1}\mathbf{D}\,\mathbf{\Lambda}, \tag{52}$$

and

$$\mathbf{G}\,\mathbf{R} = \mathbf{\Gamma}\,\mathbf{R}\,\mathbf{\Lambda}. \tag{53}$$

A new eigenvector matrix $\mathbf{R}$ is given by:

$$\mathbf{R} = \mathbf{\Gamma}^{-1}\mathbf{D} = \mathbf{F^q}\,\mathbf{D} = \left(\mathbf{D}^{-1}\right)^\dagger \mathbf{K}. \tag{54}$$

Zou and co-workers partitioned the matrices $\mathbf{\Gamma}$ and $\mathbf{G}$ into diagonal ($\mathbf{\Gamma}_d$ and $\mathbf{G}_d$) and off-diagonal parts ($\mathbf{\Gamma}_{od}$ and $\mathbf{G}_{od}$)[166]:.

$$\left(\mathbf{G}_d + \lambda\,\mathbf{G}_{od}\right)\mathbf{R}_\lambda = \left(\mathbf{\Gamma}_d + \lambda\,\mathbf{\Gamma}_{od}\right)\mathbf{R}_\lambda\mathbf{\Lambda}_\lambda. \tag{55}$$

The perturbation parameter λ in Equation (55) slowly converts the local vibrational modes, ($\lambda = 0$) adiabatically into their corresponding normal mode counterparts, ($\lambda = 1$) by slowly switching on $\mathbf{\Gamma}_{od}$ and $\mathbf{G}_{od}$, that is, by activating the mass-coupling. This one-to-one transformation between local and normal vibrational modes forms the fundamental

proof for the decomposition of normal modes into local mode contributions, opening new avenues for a comprehensive analysis of vibrational spectra.

The important question has been raised whether the Konkoli–Cremer local vibrational modes can be related to experimentally derived local modes. Figure 4a shows that local mode CH stretching frequencies ω_n^a significantly correlate ($R^2 = 0.990$) with the corresponding overtone CH stretching frequencies for a selection of organic molecules.[180–182] This demonstrates the important link between the local vibrational modes derived from normal modes (in the harmonic approximation) and the local modes derived from overtone spectroscopy. The advantage of our local modes is twofold: (a) *economic aspect*: they can be obtained from standard routine frequency calculations and measured fundamentals; (b) *fundamental aspect*: the use of overtone spectroscopy as a means of obtaining local mode information is mostly limited to terminal bonds.[67,183,184] Hence a generalization of the local mode description of chemical bonding derived from overtone spectroscopy is limited.

Figure 4b correlates McKean's experimental (*isolated*) vibrational frequencies obtained for 66 CH bonds in 38 different organic molecules via isotope substitution[139] with the corresponding calculated local mode frequencies. The set of molecules tested comprises alkanes, alkenes, alkynes, alcohols, amines, halogenated hydrocarbons, aldehydes, ketones, acids, cyanides, and so on, so that CH bonds in different hybridization states of carbon and under the impact of different substituents were represented. Due to a doubling of the hydrogen mass, frequencies for C-H/C-D stretching vibrations are significantly shifted to lower values thus eliminating a mixing with the remaining CH stretching motions. The correlation coefficient $R^2 = 0.976$ reflects good agreement with the calculated local frequencies, suggesting that isotope substitution leads to frequencies, which can be considered as experimental counterparts of the Konkoli–Cremer local vibrational frequencies. An extension of the isolated stretching frequencies to other than just XH bonds is difficult since

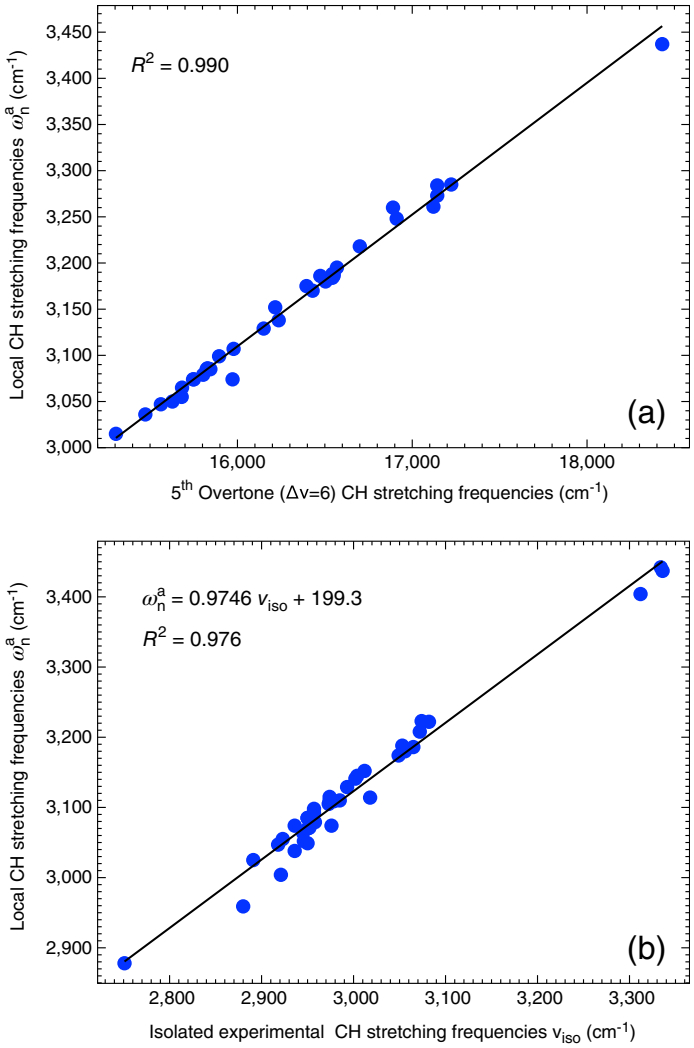

FIGURE 4 (a) Local mode versus overtone CH stretching frequencies; data was taken from Table 4.3 of Reference 32; (b) local mode versus isolated CH stretching frequencies, data was taken from Table 1 of Reference 140

a doubling of the nuclear mass is not possible for any other element frequently used in organic chemistry and because of considerable experimental efforts implied.

2.2.3 | Characterization of normal modes

In addition to local mode force constants and local mode frequencies, the local mode analysis has led to a new way of analyzing vibrational spectra. The CNM procedure decomposes each normal vibrational mode $\mathbf{l}_\mu$ into local mode contributions for a nonredundant set of N_{vib} local vibrational modes $\mathbf{a_n}$ by calculating the overlap between each local mode vector $\mathbf{a}_n^x$ with this normal mode vector $\mathbf{l}_\mu$ as $S_{n\mu}$ according to Equation (56).[38–40]

$$S_{n\mu} = \frac{\left(\mathbf{a}_n^x, \mathbf{l}_\mu\right)^2}{\left(\mathbf{a}_n^x, \mathbf{a}_n^x\right)\left(\mathbf{l}_\mu, \mathbf{l}_\mu\right)}, \tag{56}$$

where (**a**, **b**) is the scalar product of two vectors **a** and **b** including a metric

$$(\mathbf{a}, \mathbf{b}) = \sum_{i,j} a_i O_{ij} b_j. \tag{57}$$

O_{ij} is an element of the metric matrix **O**. We generally use the force constant matrix $\mathbf{F}^x$ as metric, namely $\mathbf{O} = \mathbf{F}^x$, to include the influence of the electronic structure. As derived by Konkoli and Cremer[38] the contribution of local mode $\mathbf{a}_n$ to the normal mode $\mathbf{l}_\mu$ is given by

$$C_{n\mu} = \frac{S_{n\mu}}{\sum_m^{N_{vib}} S_{m\mu}}, \tag{58}$$

that is, a completely localized normal mode $\mathbf{l}_\mu$ has a $C_{n\mu}$ value of 1 (corresponding to 100% if $C_{n\mu}$ is given as percentage). In essence, the CNM procedure complements the ACS analysis with a nonadiabatic picture, that is, a snapshot of the normal modes expressed in terms of the local mode contributions.

As an example, the ACS and CNM are shown in Figure 5 for the CH_3SCN molecule, which is a popular probe molecule for the *vibrational stark effect* (VSE). The VSE is based on Stark's original observation made in 1913, that an external electric field can cause a splitting and shifting of atomic and molecular energy levels.[188] Over the past two decades the VSE has become an important tool to measure and analyze the in situ electric field strength in various chemical environments with NIRS.[189–198] The VSE probe molecule has a characteristic bond, called *probe bond*, such as CO or CN. Assuming that the normal vibrational mode associated with the stretching frequency of the probe bond is localized and does not couple with other modes, then a shift of the probe stretching frequency directly reflects the influence of the electric field. Both ACS and CNM can assess the validity of this assumption in a quantitative way. As shown in Figure 5a, the local CN stretching frequency (left side) smoothly transforms into the corresponding normal mode frequency (right side) when turning on the mass coupling via the scaling parameter λ. In Figure 5b the corresponding decomposition of the 15 normal modes (each represented by a bar) of CH_3SCN into 15 local mode contributions is shown. As obvious from the decomposition, normal mode 12 with $\omega_\mu = 2{,}302\ \mathrm{cm}^{-1}$ has 93% local mode character, identifying CH_3SCN as suitable VSE probe. This example clearly shows the analytic potential of the local vibrational mode theory beyond characterizing the strength of chemical bonds and weak chemical interactions.

3 | RECENT EXTENSIONS

3.1 | Generalized subsystem vibrational analysis

Caused by the fact that normal vibrational modes are generally delocalized over the molecular system, it is difficult if possible at all to assign certain vibrations to specific fragments and functional groups, or to isolate the vibrations of a

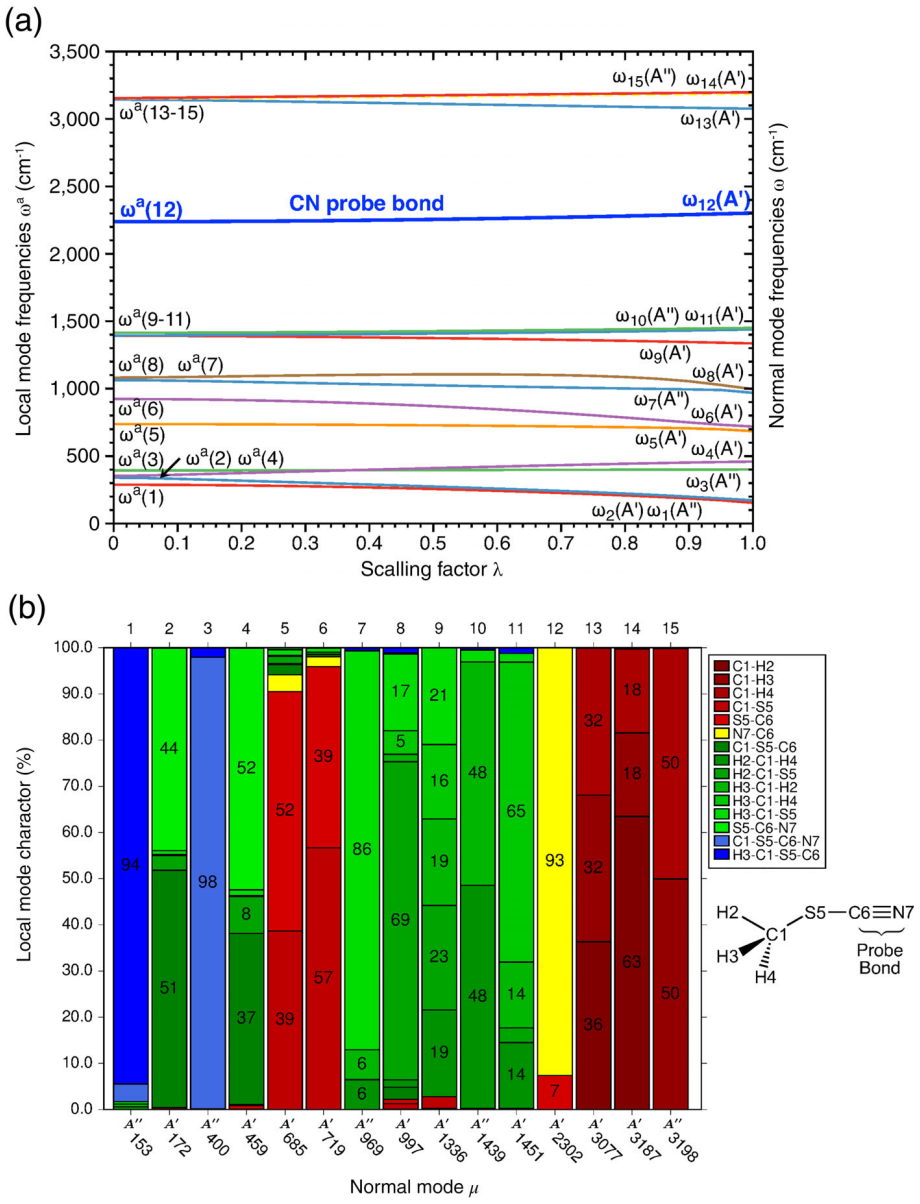

FIGURE 5 (a) Adiabatic connection scheme and (b) decomposition of normal modes into local mode contributions for CH_3SCN; ωB97X-D/aug-cc-pVDZ level of theory.[185–187]

molecule in solution or other media being described by a multilayer hybrid method, such as a mixed quantum mechanics/molecular mechanics (QM/MM) approach.[199–203] The solution to this problem requires a procedure which projects the normal vibrational modes of the total system into the targeted subsystem or fragment. Many efforts have been made to derive such a procedure, including partial Hessian diagonalization,[204] partial Hessian vibrational analysis (PHVA),[205] mobile block Hessian (MBH),[206–209] vibrational subsystem analysis (VSA),[210,211] and local Hessian transformation,[212] just to name a few. Also the unitary transformation of normal mode vectors,[152–155] mentioned in the introduction, belongs to this category. However, all these approaches share a common deficiency; the partitioning of the full Hessian matrix leads to a loss of information about the interaction between the subsystem and its environment.

Therefore, we developed a new approach, the *generalized subsystem vibrational analysis* (GSVA),[213] which avoids the partitioning of the full Hessian and instead extracts the intrinsic fragmental vibrations of any fragment/subsystem from the whole system via the evaluation of the corresponding effective Hessian matrix $\mathbf{F}^x_{sub}$ for the target subsystem of interest as outlined in Reference 213:

$$\mathbf{F}^x_{sub} = \mathbf{B}'^{\dagger}_{sub}\left(\mathbf{B}'(\mathbf{F}^x)^{+}\mathbf{B}'^{\dagger}\right)^{-1}\mathbf{B}'_{sub}, \tag{59}$$

where $\mathbf{F}^x$ is the full Hessian matrix for the whole system (i.e., subsystem plus environment) with dimension $(3N \times 3N)$. The Wilson **B**-matrix collecting a nonredundant set of $(3n - \Sigma_{sub})$ internal coordinates for the subsystem is denoted as $\mathbf{B}'$ and $\mathbf{B}'_{sub}$ in full $3N$ columns and truncated $3n$ columns (excluding the environment atoms), respectively. n is the number of atoms in the subsystem and Σ_{sub} is the total number of translations and rotations in the subsystem, (linear subsystem: $\Sigma_{sub} = 5$, nonlinear subsystem: $\Sigma_{sub} = 6$). $(\mathbf{F}^x)^+$ is the Moore–Penrose inverse[214,215] of $\mathbf{F}^x$, which is a singular matrix. $\mathbf{F}^x_{sub}$ has the dimension of $(3n \times 3n)$.

When deriving the effective Hessian matrix, the full Hessian matrix is projected into the internal vibration space of the subsystem without any need for partitioning. This is manifested in two aspects: (a) the effective Hessian matrix $\mathbf{F}^x_{sub}$ has exactly Σ_{sub} zero eigenvalues; (b) the effective Hessian matrix retains the curvature of the PES in the direction defined by any internal coordinate within the subsystem, which provides this approach with a solid physical basis. After the projection, the conventional normal mode analysis machinery can be employed using the geometry, atomic masses and the effective Hessian matrix of the subsystem for the calculation of a new type of localized normal modes. We coined these subsystem normal mode vibrations as *intrinsic fragmental vibrations*.[213] It is important to note that these intrinsic fragmental vibrations of the subsystem are transferable, that is, the intrinsic vibrations of the subsystem in one environment can be directly compared with those of the same subsystem in a different environment, for example, gas phase versus solution or solution versus inside a protein. This important feature of GSVA is discussed in the following for formaldehyde (CH_2O) in a carbon nanotube (CNT) shown in Figure 6.[213]

As described in Reference 213, the complete nonredundant parameter set for the effective Hessian matrix $\mathbf{F}^x_{sub}$ of CH_2O was composed of the three covalent bonds, two O—C—H angles, and one out-of-plane pyramidalization angle. In Table 1 the fragmental vibrational frequencies CH_2O in a CNT are compared with the corresponding normal vibrational frequencies of CH_2O in gas phase. Vibrations 3, 5, and 6 are almost unaffected by the CNT environment, with frequency differences smaller than 4 cm^{-1}. The CO stretching frequency is slightly redshifted in the CNT by 24 cm^{-1}. The largest effect was found for the symmetric and asymmetric CH stretching frequencies with blue-shifts of 79 and 70 cm^{-1}, respectively. These two motions extend into the CNT framework and therefore, respond most strongly to the confinement imposed on the formaldehyde in the CNT.

The transferability of the intrinsic fragmental vibrational frequencies can be validated via a subsequent local mode analysis. The data in Table 2 reveals that the local mode properties for the sub-system based on the effective Hessian $\mathbf{F}^x_{sub}$ and those based on the full Hessian $\mathbf{F}^x$ are identical. In summary, GSVA provides a new link between local and normal vibrational modes connecting intrinsic (subsystem) and normal mode properties.

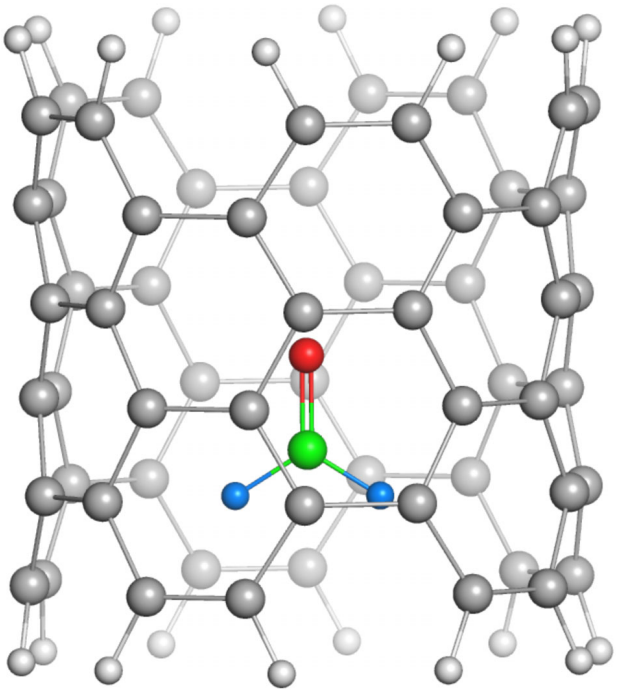

FIGURE 6 Structure of CH_2O confined in a carbon nanotube; calculated at the B3LYP level of theory[216–219] with Grimme's empirical D3 dispersion correction[220] and Becke–Johnson (BJ) damping[221] utilizing Pople's 6-31G(d,p) basis set.[222] Total number of atoms is 84. For details see Referenece [213]

TABLE 1 Intrinsic vibrational frequencies of formaldehyde in carbon nanotube (CNT) and corresponding normal mode frequencies in the gas phase in cm^{-1} as well as their characterization

No	Vib. mode	CH_2O (CNT)	CH_2O (gas phase)	Character
1	A_1	2,976	2,897	Symmetric CH stretching
2	A_1	1823	1847	CO stretching
3	A_1	1,554	1,555	In-plane scissoring of HCH angle
4	B_2	3,024	2,954	Asymmetric CH stretching
5	B_2	1,278	1,275	In plane rocking of H atoms
6	B_1	1,201	1,201	Out of plane pyramidalization

Note: For details see Reference 213.

TABLE 2 Local mode force constants $k^a_{n,sub}$ based on the effective Hessian matrix $\mathbf{F}^x_{sub}$ and local mode force constants k^a_n based on the full Hessian matrix $\mathbf{F}^x$ for formaldehyde

Local vib. mode	q_n	$k^a_{n,sub}$	k^a_n
1	R(CO)	13.306	13.306
2	R(CH)	4.924	4.924
3	R(CH)	4.918	4.918
4	α(OCH)	1.109	1.109
5	α(OCH)	1.110	1.110
6	$\mathcal{P}$ (C′—O—H—H)	3.496	3.496

Note: q_n defines the internal coordinate being associated with local mode a_n. R denotes bond stretching (unit: mdyn/Å), α angle bending (unit: mdyn Å/rad^2), and $\mathcal{P}$ out-of-plane pyramidalization (unit: mdyn Å/rad^2), where the primed C atom moves out of the plane defined by the following three atoms. For calculational details see Reference 213.

3.2 | Periodic local modes for crystals and solids

After successfully studying the intrinsic strength of chemical bonds and weak chemical interactions in single molecules and molecular complexes (which will be discussed in more detail in Section 4) we recently extended the local mode theory from molecular to periodic systems and crystals with a particular focus on local mode force constants. The major objective of this work was to develop a method leading to a deeper understanding of crystal bonding and allow for a direct comparison of the intrinsic bond strength in periodic and molecular systems.[223]

As outlined in Reference 223, a necessary prerequisite for this extension was to consider the major differences of single molecule and solid state vibrational spectroscopy: (a) While a single molecule has always N_{vib} vibrational frequencies, in periodic systems the number of vibrations depends on the dimensionality, that is, $(3N - 4)$ for one-dimensional periodic systems and $(3N - 3)$ for two- and three-dimensional periodic systems, with N being the number of atoms in the primitive cell.[142] (b) Periodic systems may have multiple sets of vibrational frequencies depending on the wave vector $\mathbf{q}$ within the phonon dispersion spectrum, whereas there is one and only one set of vibrational frequencies for a molecular systems.[224] (c) Only the set of frequencies can be measured by infrared and Raman spectroscopy, which is taken at the $\mathbf{\Gamma}$-point, $(\mathbf{q} = \mathbf{0})$[225–227] where $\mathbf{q}$ defines points of the irreducible Brillouin zones.[141] Therefore, we derived the local vibrational modes at the $\mathbf{\Gamma}$-point, forming the basis for a direct comparison of molecular vibrations and their periodic counterparts. Another benefit of doing so is that the lattice vibrations at the $\mathbf{\Gamma}$-point correspond to the vibrations of the primitive cell, which is the smallest unit cell with translational symmetry.[141] This allows us to restrict the calculation of the force constant matrix to the primitive cell model and qualifies local mode properties in periodic systems as being independent of the choice of primitive cell.[223]

As outlined in Reference 223 we define a local vibrational mode in a periodic system as a vibration initiated by a specific internal coordinate q_n (e.g., a bond length) in all primitive cells while all other parts of the periodic system relax. This definition allows for the direct comparison of the intrinsic strength of a bond characterized by the local mode force constant in periodic and molecular systems. In the following we will summarize the derivation of the local mode force constant k^a_n in periodic systems, a more detailed discussion is given in Reference 223.

Given a primitive cell containing N atoms and its force constant matrix $\mathbf{F}_p^x$ in Cartesian coordinates, the N_{vib} non-zero eigenvalues of $\mathbf{F}_p^x$ are collected in a diagonal matrix $\boldsymbol{\Lambda}'$

$$\mathbf{F}_p^x \mathbf{V} = \mathbf{V}\boldsymbol{\Lambda}', \tag{60}$$

where $N_{vib} = 3N - 4$ for one-dimensional periodic systems (i.e., linear polymers) or $N_{vib} = 3N - 3$ for two-dimensional periodic systems (i.e., slabs) and three-dimensional systems (i.e., solids). Matrix $\mathbf{V}$ collects N_{vib} eigenvectors $\mathbf{v}_\mu$ in columns. Equation (60) can be rewritten as

$$\boldsymbol{\Lambda}' = \mathbf{V}^\dagger \mathbf{F}_p^x \mathbf{V}. \tag{61}$$

The $\mathbf{d}'_n$ vector associated with a specific internal coordinate q_n in the primitive cell is then calculated in analogy to Equation (13)

$$\mathbf{d}'_n = \mathbf{B}_n \mathbf{V}, \tag{62}$$

where $\mathbf{B}_n$ is the Wilson **B**-matrix for the internal coordinate q_n. Then, the local mode force constant k_n^a in the primitive cell is calculated by

$$k_n^a = \left(\mathbf{d}'_n (\boldsymbol{\Lambda}')^{-1} \mathbf{d}'^{\dagger}_n\right)^{-1}, \tag{63}$$

which is analogous to Equation (43).

One of the examples presented in Reference 223 concerns the comparison of CC bonds in molecules and solid material. In Table 3 and Figure 7 the CC bond strength of some representative hydrocarbon molecules is compared with that of the CC bonds in 2D-graphene sheets and solid 3D-diamond. It has been suggested in the literature that the CC bond strength in graphene is in between that of the C—C single bond in ethane and that of the C═C double bond in ethylene, based on the fact that in addition to forming three σ bonds with neighboring carbons each sp^2 hybridized C atom in graphene has one electron in its p orbital perpendicular to the 2D plane forming an extended π-bond being delocalized over the whole system.[228–232] The local mode analysis could for the first time rigorously quantify this suggestion via a direct comparison of local CC force constants and related BSO n values. Compared with the CC bonds in ethane and ethylene, the CC bonds in graphene are in between those two references with regard to both, the bond length and bond strength as shown in Figure 7. The graphene CC bond is 0.027 Å longer than the aromatic CC bond in benzene. It is also weaker, as reflected by the local mode force constant; 1.228 mdyn/Å in graphene versus 1.462 mdyn/Å in benzene. In addition, more specific details could be disclosed. Although both graphene and benzene share a C_6 ring topology, the

TABLE 3 CC Bond length R(CC) in Å, local CC force constants k^a in mdyn/Å and corresponding bond strength orders BSO n for representative hydrocarbons, molecules (**1**–**6**), a 2D-graphene layer (**7**), and solid 3D-diamond (**8**)

#	Molecule/system	R(CC)	k^a	BSO n
1	Ethane	1.535	4.011	1
2	Ethylene	1.336	9.527	2
3	Acetylene	1.212	16.923	3.169
4	1,3,5-Hexatriene (C-C)	1.449	5.200	1.231
5	Benzene	1.402	6.446	1.462
6	Naphthalene	1.441	5.248	1.274
7	Graphene	1.429	5.182	1.228
8	Diamond	1.552	3.554	0.907

Note: All 8 systems were modeled at the TPSS/6-31G(d,p) level. In addition, periodic boundary conditions were employed for (**7**) and (**8**).[223]

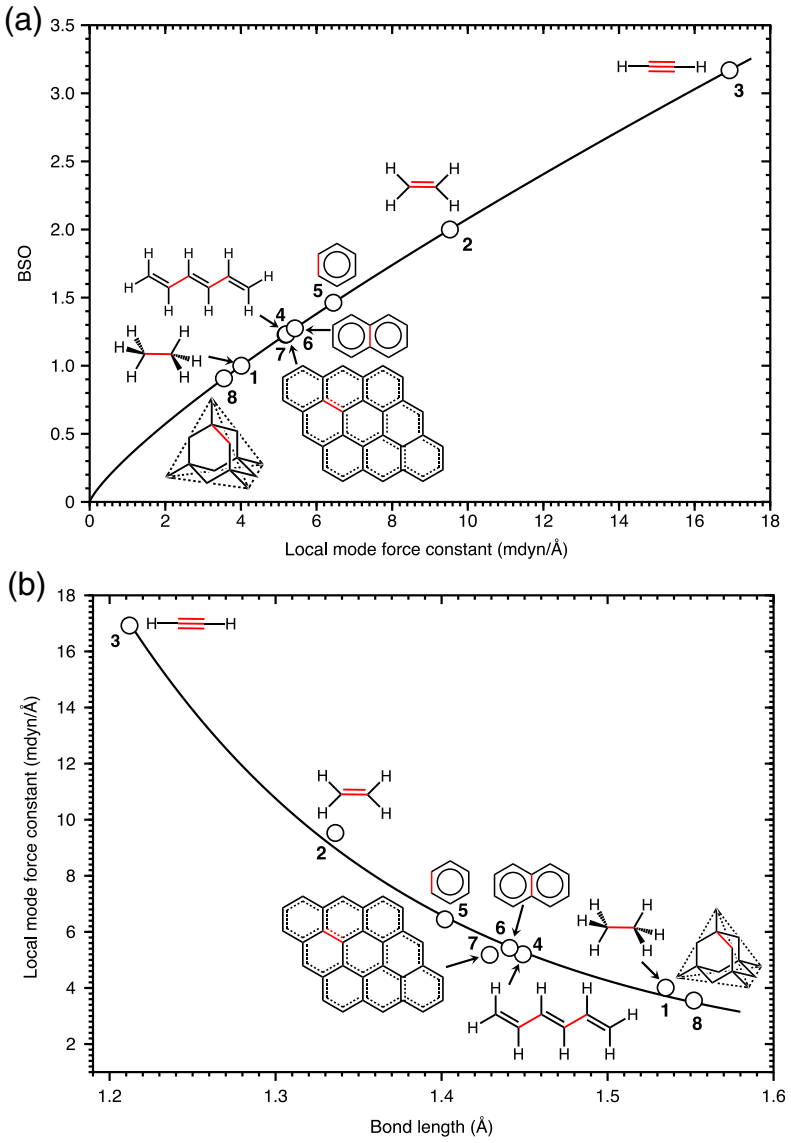

FIGURE 7 (a) BSO (CC) determined from local CC force constants using Equations (44)–(45). (b) Correlation between CC bond lengths and local force constants. CC bonds analyzed are marked in red. For calculational details see Reference 223

π electrons in graphene delocalize over a larger space, thus leading to weaker CC bonds, which is already indicated for the CC bond of naphthalene. As shown in Table 3, the CC bond strength in graphene (BSO $n = 1.228$) is close to that of the single bond in 1,3,5-hexatriene, (BSO $n = 1.231$).

Diamond is one of the hardest natural materials,[233] which could lead to the assumption that it has one of the strongest CC bonds. However, our local mode analysis identified the CC bond in diamond as the weakest among the CC bonds presented in Table 3 and in Figure 7.[223] Each carbon atom in diamond adopts sp^3 hybridization leading to a tetrahedral configuration like in the case of ethane.[234] However, the diamond CC bond is longer than the ethane CC single bond and its local stretching force constant is smaller by 0.457 mdyn/Å (see Table 3), in line with CC bond energies of 88 kcal/mol for the CC bond in ethane[235] and 62 kcal/mol for the CC bond in diamond.[236]

The major difference is that in diamond each C atom is surrounded by four C atoms while the C atoms in ethane are surrounded by one C and three H atoms. Compared with the carbon atoms in diamond, the hydrogen atoms in ethane are less capable of attracting bonding electrons, and in this way moving them out of the CC bond region.[237] As for the hardness of diamond not a single CC bond but the large network of covalent CC bonds matters.[237,238] This example shows how we can quantify the intrinsic bond strengths of CC bonds in 2D graphene as well as 3D diamond and rank them among a series of hydrocarbons. Such an analysis could also be useful to quantify the CC bond strength in other carbon allotropes,[237,239] e.g., in CNTs.[240] As CNTs can be made with a variety of different structures, the characterization of the CC bond strength in CNTs will be an interesting direction to pursue.

4 | APPLICATIONS

As summarized in Table 4 the local mode theory has been successfully applied to characterize covalent bonds and weak chemical interactions such as hydrogen, halogen, chalcogen, pnicogen, and tetrel bonding, as well as BH···π interactions. Existing concepts could be generalized such as the Badger rule, new electronic descriptors were developed such as a new aromaticity index based on local mode force constants as well as a new descriptor of metal ligand bond strength. Some highlights are described in the following.

The ongoing debate about a C_2 quadruple bond[290–293] could be brought to a successful end.[167] In comparison with the local CC stretching force constants and corresponding BSO n values of ethane, ethene, and acetylene, the intrinsic CC bond strength of C_2 in its $^1\Sigma_g^+$ ground state was determined to be half way between that of a double bond and that of a triple bond.

Based on a fruitful combination of quantum chemical predictions and experimental realization, for the first time, nonclassical H-bonding involving a BH···π interaction could be identified.[268,269] According to the Cremer–Kraka criteria for covalent bonding,[294,295] this interaction is electrostatic in nature with a BSO n of 0.35, being comparable to what we found for the H-bond in the water dimer.[174,250]

A method for the quantitative assessment of aromaticity and anti-aromaticity, based on vibrational spectroscopy was developed,[270] which led to a new understanding of Clar's rule.[296] The analysis of 30 mono- and polycyclic conjugated hydrocarbons confirmed Clar's rule of disjoint benzene units in many cases, but corrects it in those cases where peripheral π-delocalization leads to greater stability. The structure and stability of polycyclic gold clusters, based on a new Clar's aromaticity rule equivalent for metal–metal bonds, could be rationalized for the first time.[271]

Modeling of liquid water clusters with 50 and 1,000 water molecules at different temperatures using quantum mechanical and MD simulations, respectively led to a series of interesting results.[251,252] As shown in Figure 8 each water molecule can usually accept/donate at most 2 hydrogen bonds leading to a variety of different hydrogen bond combinations. MD calculations identified ca. 2 million hydrogen bonds in these water clusters belonging to 16 different

TABLE 4 Successful applications of the local vibrational mode theory

Topic	References
Covalent bonds	
The strongest bond in chemistry	167,169,241
Long carbon–carbon bonds	242
Carbon-halogen bonds	243,244
Generalized Badger rule, bond strength bond length relation	32,140,168,245–248
Weak chemical interactions	
Hydrogen bonding	174,175,249–255
Halogen bonding	253,255–261
Pnicogen bonding	262–264
Chalcogen bonding	247,265,266
Tetrel bonding	267
BH···π interactions	268,269
New electronic descriptors	
Aromaticity index	270–272
Metal electronic parameter	254,258,271,273–276
Additional topics	
Chemical similarity	277,278
Molecular acidity (pK_a)	279
Chiral discrimination	280
Unified reaction valley approach (URVA) and local modes	281–287
Force field parameters	288
Local modes for periodic systems	223,289

types of hydrogen bonds with different strength, as shown in Figure 8. In warm water, the weaker hydrogen bonds with predominantly electrostatic contributions are broken, smaller water clusters with strong hydrogen bonding arrangements remain. These cluster units can easily rearrange to form the hexagonal lattice of ice as sketched in Figure 8.

In cold water, many weak four-coordinated hydrogen bonds exist which need to be first broken before forming the ice lattice, which costs energy and time delaying the freezing process. Therefore, warm water freezes faster than cold water. This effect known in the literature as the *Mpemba effect*, according to its discovery by Mpemba in 1969,[297] could now for the first time be explained at the atomistic level utilizing our local mode analysis.[251,298]

The local mode analysis has led to a new quantitative measure of metal–ligand (M–L) bonding, the metal ligand electronic parameter (MLEP),[254,258,271,273–276] work that was inspired by Tolman's electronic parameter TEP.[299–301] The TEP has been used by experimentalists over the past decades as a popular measure describing the strength of a M–L bond, in particular in connection with transition-metal catalysis, (for a comprehensive literature overview, see Table 3 in Reference 275). Tolman's experimentally derived TEPs were complemented by computationally derived counterparts, the so-called CEPs.[302–308] Both TEP and the corresponding CEP are indirect bond strength measures being originally defined as the A_1-symmetrical CO stretching frequency of nickel tricarbonyl phosphine complexes of the type L—Ni$(CO)_3$, L = R_3P with (pseudo)-C_{3v} symmetry.[299–301] Tolman used the A_1-symmetrical CO stretching frequency because it could be easily identified in an infrared spectrum, recorded with the instruments of the 1960s, whereas the M–L stretching frequency was out of reach. He assumed that the carbonyl ligand reflects indirectly how the ligand L influences the electronic structure at the metal atom, and in this way M–L bonding. Tolman's line of argument was that any ligand L increasing the electron density at the metal atom causes a transfer of negative charge from the d-orbitals of Ni into in the low-lying π^* (CO) orbitals. As a consequence, the CO bond becomes weaker and the A_1-symmetrical CO stretching frequency is red-shifted. This redshift is registered within the infrared spectrum and qualifies the TEP as an indirect descriptor for the metal–ligand bond strength. He further assumed that (a) the A_1-symmetrical CO stretching

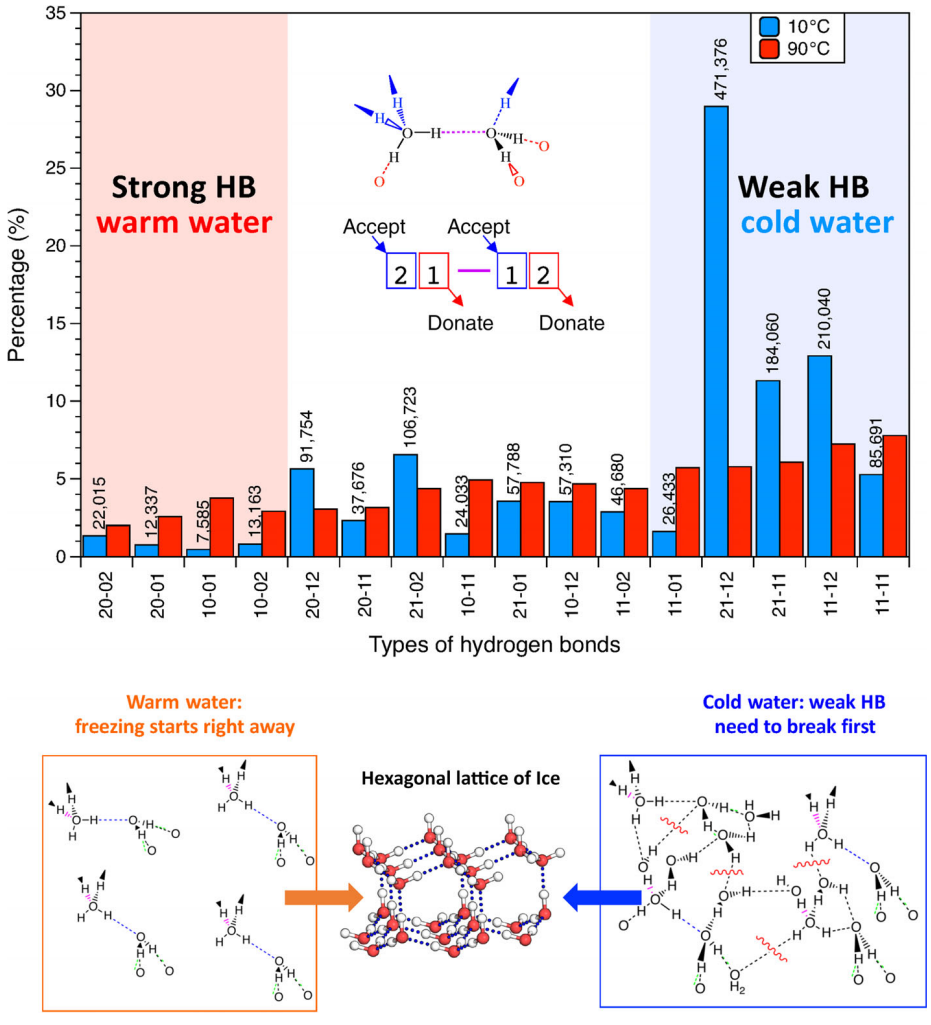

FIGURE 8 Upper panel: Frequency of 16 different types of hydrogen bonds (BHs) (in %) found in the molecular dynamics simulations (MDS) of $(H_2O)_{1,000}$. The MDS simulations were carried out at two different temperatures to simulate warm water (90°C; red bars) and cold water (10°C; blue bars). The insert illustrates the four-digit notation applied to identify the different hydrogen bond types. Lower panel: Explanation of the Mpemba effect.[251]

frequency does not couple with other vibrational modes and (b) that the A_1-symmetrical CO stretching frequency correlates with the M–L bond strength. By utilizing the local mode theory, we could for the first time assess the validity of these important assumptions. Based on an intensive local mode analysis of ca. 200 nickel-tricarbonyl complexes we could show that the TEP is at best a qualitative parameter, suffering from relatively large mode-mode coupling errors (in the range of 100 cm^{-1}).[273,275] Furthermore, we unravelled the basic problem that the A_1-symmetrical CO stretching frequency correlates with the intrinsic M–L bond strength if at all only within a small set of similar compounds. There is also no direct relationship between the intrinsic M–L bond strength and the local CO stretching frequency, which is free from any mode-mode coupling.[273–275] Therefore, it is more efficient to assess the catalytic activity of transition metal complexes $(R)_nM - L$ directly from the metal–ligand electronic parameter (MLEP), which we define as the local stretching force constant of the M–L bond or the related BSO n.[273,275] In Tolman's defense it has to be pointed out that he had to choose the A_1-symmetrical CO stretching frequency, because of instrumental limitations. However, modern advanced Terahertz spectroscopy[5,12,309–311] can record far infrared absorptions down to 40 cm^{-1} which easily includes the range of the M–L stretching frequencies. The MLEP assesses both electronic and steric factors in a quantitative way and therefore forms the ideal basis for a collection of M–L bond strength parameters across the periodic table. In addition, the MLEP can be determined for any metal or transition metal complex whether it contains CO ligands or not.[273–275] So far we have introduced MLEPs for Pb, Ti, Cr ligand bonds,[274] Au—Au interactions,[271] and Fe—H bonding,[254] which is discussed in more detail in the following.

In connection with a recent study of the trans-effect of different ligands L on Fe—H_2 and Fe—H^- bonding of a [NiFe] hydrogenase mimic, Makoś and co-workers introduced the MLEP for Fe—H bonds.[254] 17 different ligands L were applied including π-donor ligands such as Cl^-, F^-, and OH^-, σ-donor ligands such as CH_3^-, $C_2H_5^-$, NH_3 and σ-donor/π-acceptor ligands such as CN^- and CO. Figure 9 shows that the BSO(FeH) values of the compounds studied in this work range between 0.4 and 0.65. As expected, the iron-hydride bonds in complexes **B1**–**B17** are stronger than their Fe—H_2 counterparts in complexes **A1**–**A17**. It is interesting to note that in the case of the Fe—H_2 interactions, the Fe—H_a bonds turned out to be generally weaker than Fe—H_b bonds in complexes **A1**–**A17**,[254] although the Fe—H_b bond is the bond to be broken when complex **A** transforms into **B**, which is currently under further investigation.

As revealed by the results presented in Reference 254, Fe—H interactions are weakened by σ-donor/π-acceptor ligands while strengthened by σ-donor or π-donor ligands. The opposite is true for the H—H bond of H_2. It is weakened by σ-donor or π-donor ligands while strengthened by σ-donor/π-acceptor ligands. These findings form a valuable basis

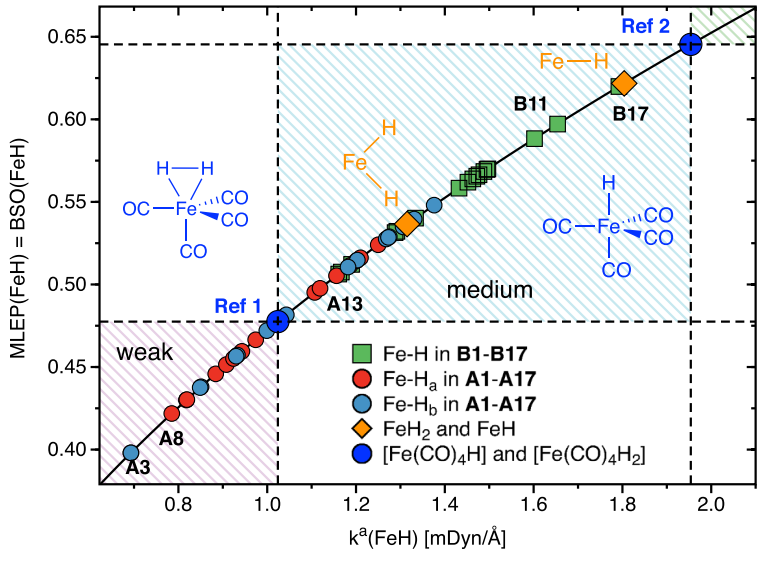

Ligand	SCN^-	CO	NO_2^-	CN^-	PH_3	ON	CH_3^-	$C_6H_5^-$	$C_2H_5^-$	C_2H_4	NH_3	H_2S	NCS^-	F^-	Cl^-	OH^-	H_2O
Complex **A**	A1	A2	A3	A4	A5	A6	A7	A8	A9	A10	A11	A12	A13	A14	A15	A16	A17
Complex **B**	B1	B2	B3	B4	B5	B6	B7	B8	B9	B10	B11	B12	B13	B14	B15	B16	B17

FIGURE 9 MLEP(FeH) = BSO(FeH) for Fe—H and Fe—H_2 derived from the local FeH stretching force constants k_n^a (FeH) via Equations (44)–(46). Low-spin $Fe(CO)_5$ was used as the reference molecule, in which one axial CO ligand was replaced by H_2 ([1]) and H^- ([2]), respectively. (Reprinted with permission from Reference 254. Copyright 2019 from Springer Nature)

for future catalyst design based on [NiFe] hydrogenase mimics and for systematic design of new biomimetic catalysts for H_2 generation. The MLEP(Fe-H) can also be applied more broadly. Figure 9 includes two iron hydrides, the high spin FeH_2 molecule, the only transition metal dihydride, which has been detected in the gas phase,[312] and the diatomic FeH molecule, which has attracted a lot of attention in astrochemistry being one of the few molecules identified in the sun.[313,314]

It is interesting to note that the Fe—H bond of the lowest-lying $X^4\Delta$ state of FeH is as strong as the strongest NiFe complex B17. This example shows the potential of the new MLEP(Fe—H) for the exploration of FeH bonding and the design of new functional materials based on metal hydrides.[315,316]

5 | CONCLUSIONS

In this article the local mode theory of Konkoli and Cremer was reviewed. It was shown that (a) the local mode theory furnishes bond strength descriptors derived from force constant matrices with a physical basis, (b) provides the long-searched-for extension of the Badger rule to polyatomic molecules, (c) and offers a simpler way to derive localized vibrations in chemically relevant coordinates than via the complex route of overtone spectroscopy. Therefore, one can say that the local mode theory bridges and unifies earlier attempts to obtain straightforward and easy to interpret chemical information from vibrational spectroscopy.

Special features of the local mode theory which were discussed include:

- The local vibrational modes of Konkoli and Cremer can be directly derived from the fundamental normal modes (obtained in the harmonic approximation of the potential energy) via mass-decoupled Euler–Lagrange equations.
- There is a 1:1 relationship between the normal vibrational modes and a complete, nonredundant set of local vibrational modes via an ACS. This relationship forms the basis for the decomposition of each normal mode into local mode contributions (analysis of vibrational spectra).
- The local mode analysis can also be applied to experimentally derived vibrational frequencies within the framework of the harmonic approximation of the potential energy.
- In contrast to compliance constants being derived from the inverse of the force constant matrix in internal coordinates,[100] each local mode force constant is assigned with a local vibrational mode, local mode frequency, mass, and other local properties. No time-consuming Hessian matrix inversion is needed which is an important advantage for the investigation of large systems.
- Local mode stretching force constants are directly related to the intrinsic strength of a bond and therefore, provide a unique measure of bond strength based on vibrational spectroscopy.
- Local mode properties of molecules and periodic systems can be directly compared.

An overview of the great potential of the local mode theory was given, highlighting its successful application to characterize covalent bonds (e.g., identifying the strongest and weakest covalent chemical bonds currently known in chemistry) and weak chemical interactions such as hydrogen, halogen, chalcogen, pnicogen, and tetrel bonding, as well as atom$\cdots\pi$ interactions. New electronic descriptors such as a generalized Badger rule, a new aromaticity index and a new metal–ligand electronic parameter, both being based on vibrational spectroscopy were discussed. We also showed how the characterization of normal mode (CNM) procedure, which decomposes each vibrational normal mode into local mode contributions can be used as an efficient tool to assess the validity of a VSE probe; and introduced the seamless extension of the local mode analysis from molecular to periodic systems. Our vision is that in the future the local mode analysis will be routinely applied by the computational community like the natural bond orbital analysis.[317,318]

ACKNOWLEDGMENTS

This review is dedicated to Dieter Cremer (1944-2017) who laid the foundation for the local vibrational mode theory and its success. We thank James J. Turner, Vytor P. Oliveira, Alexis Delgado, and Seth Yannacone for fruitful discussions and suggestions. This work was financially supported by the National Science Foundation (Grant CHE 1464906). We thank SMU for providing generous computational resources. W. Z. also acknowledges the financial support by National Natural Science Foundation of China (Grant No. 21673175) and the Double First-Class University Construction Project of Northwest University.

CONFLICT OF INTEREST

The authors have declared no conflicts of interest for this article.

AUTHOR CONTRIBUTIONS

Elfi Kraka: Conceptualization; methodology; validation; writing-original draft, writing-review and editing; supervision. Wenli Zou: Conceptualization; methodology; data curation; validation; visualization; writing-review and editing. **Yunwen Tao:** Conceptualization; data curation; methodology; validation; visualization; writing-review and editing.

ORCID

Elfi Kraka https://orcid.org/0000-0002-9658-5626

RELATED WIREs ARTICLE

Local modes in vibration-rotation spectroscopy

REFERENCES

1. Larkin P. *Infrared and Raman Spectroscopy: Principles and Spectral Interpretation*. Amsterdam, Netherlands: Elsevier Science, 2017.
2. Thompson JM. *Infrared Spectroscopy*. Singapore: Jenny Stanford Publishing, 2018.
3. Smith E, Dent G. *Modern Raman Spectroscopy: A Practical Approach*. New York, NY: Wiley, 2019.
4. Wu G. *Vibrational Spectroscopy*. Berlin, Germany: De Gruyter, 2019.
5. Coutaz JL, Garet F, Wallace VP. *Principles of Terahertz Time-Domain Spectroscopy: An Introductory Textbook*. Singapore: Jenny Stanford Publishing, 2018.
6. Parker SF, Ramirez-Cuesta AJ, Daemen L. Vibrational spectroscopy with neutrons: recent developments. *Spectrochim Acta A*. 2018;*190*:518–523.
7. Silva C, Braz A, Pimentel MF. Vibrational spectroscopy and chemometrics in forensic chemistry: critical review, current trends and challenges. *J Braz Chem Soc*. 2019;*30*:2259–2290.
8. Laane J. *Frontiers and Advances in Molecular Spectroscopy*. Amsterdam, Netherlands: Elsevier Science, 2017.
9. Beć KB, Huck CW. Breakthrough potential in near-infrared spectroscopy: Spectra simulation. A review of recent developments. *Front Chem*. 2019;*7*:48–1–48–22.
10. Puzzarini C, Bloino J, Tasinato N, Barone V. Accuracy and interpretability: the devil and the holy grail. New routes across old boundaries in computational spectroscopy. *Chem Rev*. 2019;*119*(13):8131–8191.
11. You S, Lü JT, Guo J, Jiang Y. Recent advances in inelastic electron tunneling spectroscopy. *Adv Phys*. 2017;*2*(3):907–936.
12. Huang Y, Chang C, Yuan J, Zhao Z. High-harmonic and terahertz spectroscopy (HATS): methods and applications. *Appl Sci*. 2019;*9*(5):853.
13. Quaresima V, Ferrari M. A mini-review on functional near-infrared spectroscopy (fNIRS): where do we stand, and where should we go? *Photonics*. 2019;*6*(3):87.
14. Nafie LA. Recent advances in linear and nonlinear Raman spectroscopy. Part XIII. *J Raman Spectrosc*. 2019;*50*(12):1783–1806.
15. Silver A, Kitadai H, Liu H, et al. Chemical and bio sensing using graphene-enhanced Raman spectroscopy. *Nanomaterials*. 2019;*9*(4):516.
16. Downes A. Wide area Raman spectroscopy. *Appl Spectrosc Rev*. 2019;*54*(5):445–456.
17. Shao F, Zenobi R. Tip-enhanced Raman spectroscopy: principles, practice, and applications to nanospectroscopic imaging of 2D materials. *Anal Bioanal Chem*. 2019;*411*(1):37–61.
18. Yamada Y, Suzuki H, Yamashita Y. Time-domain near-infrared spectroscopy and imaging: A review. *Appl Sci*. 2019;*9*(6):1127.
19. Rohringer N. X-ray Raman scattering: a building block for nonlinear spectroscopy. *Philos Trans R Soc A*. 2019;*377*(2145):20170471.
20. Hansen AS, Vogt E, Kjaergaard HG. Gibbs energy of complex formation—combining infrared spectroscopy and vibrational theory. *Int Rev Phys Chem*. 2019;*38*(1):115–148.
21. Kiefer LM, Kubarych KJ. Two-dimensional infrared spectroscopy of coordination complexes: from solvent dynamics to photocatalysis. *Coord Chem Rev*. 2018;*372*:153–178.
22. Teixeira AM, Sousa C. A review on the application of vibrational spectroscopy to the chemistry of nuts. *Food Chem*. 2019;*277*:713–724.
23. Alula MT, Mengesha ZT, Mwenesongole E. Advances in surface-enhanced Raman spectroscopy for analysis of pharmaceuticals: a review. *Vib Spectrosc*. 2018;*98*:50–63.
24. Pahlow S, Weber K, Popp J, et al. Application of vibrational spectroscopy and imaging to point-of-care medicine: a review. *Appl Spectrosc*. 2018;*72*(S1):52–84.
25. Ewing AV, Kazarian SG. Recent advances in the applications of vibrational spectroscopic imaging and mapping to pharmaceutical formulations. *Spectrochim Acta A*. 2018;*197*:10–29.
26. O'Dea D, Lyng FM, Nicholson S, O'Connell F, Maguire A, Malkin A. Recent advances in the vibrational spectroscopic diagnosis of non-small cell lung cancer. *Vib Spectrosc*. 2019;*104*:102946.

27. Jamieson LE, Byrne HJ. Vibrational spectroscopy as a tool for studying drug-cell interaction: could high throughput vibrational spectroscopic screening improve drug development? *Vib Spectrosc*. 2017;*91*:16–30.
28. Perez-Guaita D, Kochan K, Martin M, et al. Multimodal vibrational imaging of cells. *Vib Spectrosc*. 2017;*91*:46–58.
29. Chen C, Liu W, Tian S, Hong T. Novel surface-enhanced Raman spectroscopy techniques for DNA. *Protein Drug Detection Sens*. 2019;*19*(7):1712.
30. Christensen D, Rüther A, Kochan K, Pérez-Guaita D, Wood B. Whole-organism analysis by vibrational spectroscopy. *Annu Rev Anal Chem*. 2019;*12*(1):89–108.
31. Shipp DW, Sinjab F, Notingher I. Raman spectroscopy: techniques and applications in the life sciences. *Adv Opt Photonics*. 2017;*9*(2):315.
32. Kraka E, Larsson JA, Cremer D. Generalization of the badger rule based on the use of adiabatic vibrational modes. In: Grunenberg J, editor. *Computational Spectroscopy*. New York, NY: Wiley, 2010; p. 105–149.
33. Badger RM. A relation between internuclear distances and bond force constants. *J Chem Phys*. 1934;*2*:128–131.
34. Wilson EB, Decius JC, Cross PC. *Molecular Vibrations*. New York, NY: McGraw-Hill, 1955.
35. Herzberg G. *Molecular Spectra and Molecular Structure. II. Infrared and Raman Spectra of Polyatomic Molecules*. New York, NY: Van Nostrand, 1945.
36. Konkoli Z, Cremer D. A new way of analyzing vibrational spectra. I. Derivation of adiabatic internal modes. *Int J Quant Chem*. 1998;*67*:1–9.
37. Konkoli Z, Larsson JA, Cremer D. A new way of analyzing vibrational spectra. II. Comparison of internal mode frequencies. *Int J Quant Chem*. 1998;*67*:11–27.
38. Konkoli Z, Cremer D. A new way of analyzing vibrational spectra. III. Characterization of normal vibrational modes in terms of internal vibrational modes. *Int J Quant Chem*. 1998;*67*:29–40.
39. Konkoli Z, Larsson JA, Cremer D. A new way of analyzing vibrational spectra. IV. Application and testing of adiabatic modes within the concept of the characterization of normal modes. *Int J Quant Chem*. 1998;*67*:41–55.
40. Cremer D, Larsson JA, Kraka E. New developments in the analysis of vibrational spectra on the use of adiabatic internal vibrational modes. In: Parkanyi C, editor. *Theoretical and Computational Chemistry*. Amsterdam, Netherlands: Elsevier, 1998; p. 259–327.
41. Ellis JW. Heats of linkage of C—H and N—H bonds from vibration spectra. *Phys Rev*. 1929;*33*:27–36.
42. Timm B, Mecke R. Quantitative absorptionsmessungen an den CH-oberschwingungen einfacher kohlenwasserstoffe. *Z Physik*. 1935;*98*(5–6):363–381.
43. Gänswein P, Mecke R. Absorptionsuntersuchungen an Kohlenwasserstoffen im nahen Ultraroten. *Z Physik*. 1936;*99*(3–4):189–203.
44. Vierling O, Mecke R. Absorptionsuntersuchungen an Kohlenwasserstoffen im nahen ultraroten. *Z Physik*. 1936;*99*(3–4):204–216.
45. Lippert E, Mecke R. Spektroskopische Konstitutionsbestimmungen aus ultraroten Intensitätsmessungen an CH-Schwingungsbanden. *Z Elektrochem*. 1951;*55*:366–374.
46. Lüttke W, Nonnenmacher GAA. Reinhard Mecke (1895–1969): scientific work and personality. *J Mol Struct*. 1995;*347*:1–18.
47. Darling BT, Dennison DM. The water vapor molecule. *Phys Rev*. 1940;*57*:128–139.
48. Henry BR, Siebrand W. Anharmonicity in polyatomic molecules. The CH-stretching overtone spectrum of benzene. *J Chem Phys*. 1968;*49*:5369.
49. Hayward RJ, Henry BR. A general local-mode theory for high energy polyatomic overtone spectra and application to dichloromethane. *J Mol Spectrosc*. 1975;*57*:221–235.
50. Henry BR. The local mode model and overtone spectra: A probe of molecular structure and conformation. *Acc Chem Res*. 1987;*20*:429–435.
51. Rong Z, Henry BR, Robinson TW, Kjaergaard HG. Absolute intensities of CH stretching overtones in alkenes. *J Phys Chem A*. 2005;*109*:1033–1041.
52. Kjaergaard HG, Yu H, Schattka BJ, Henry BR, Tarr AW. Intensities in local mode overtone spectra: propane. *J Chem Phys*. 1990;*93*:6239–6248.
53. Kjaergaard HG, Turnbull DM, Henry BR. Intensities of CH- and CD-stretching overtones in 1,3-butadiene and 1,3-butadiene-d_6. *J Chem Phys*. 1993;*99*:9438–9452.
54. Sibert EL III. Modeling vibrational anharmonicity in infrared spectra of high frequency vibrations of polyatomic molecules. *J Chem Phys*. 2019;*150*(090901):1–16.
55. Lawton RT, Child MS. Excited stretching vibrations of water: The quantum mechanical picture. *Mol Phys*. 1980;*40*:773–792.
56. Lawton RT, Child MS. Local and normal stretching vibrational states of H_2O. Classical and semiclassical considerations. *Mol Phys*. 1981;*44*:709–723.
57. Child MS, Lawton RT. Local and normal vibrational states: a harmonically coupled anharmonic-oscillator model. *Faraday Discuss Chem Soc*. 1981;*71*:273–285.
58. Connor JNL. The scientific life of mark sheard child. *Mol Phys*. 2006;*104*:3–9.
59. Lehmann KK. On the relation of child and Lawton's harmonically coupled anharmonic-oscillator model and Darling–Dennison coupling. *J Chem Phys*. 1983;*79*:1098.
60. Lehmann KK. On the relationship of normal modes to local modes in the vibrations of D_{6h} symmetry molecules. *J Chem Phys*. 1986;*84*:6524–6525.
61. Mills IM, Robiette AG. On the relationship of normal modes to local modes in molecular vibrations. *Mol Phys*. 1985;*56*:743–765.

62. Baggott JE. Normal modes and local modes in H_2X: beyond the *x*, *K* relations. *Mol Phys*. 1988;*65*:739–749.
63. Law MM, Duncan JL. Anharmonic stretching vibrations expressed as local modes. *Mol Phys*. 1998;*93*:809–819.
64. Law MM, Duncan JL. Anharmonically-coupled local mode to normal mode Hamiltonian transformations: Beyond the x, K-relations. *Mol Phys*. 1998;*93*:821–830.
65. Matthews DA, Vazquez J, Stanton JF. Calculated stretching overtone levels and Darling–Dennison resonances in water: A triumph of simple theoretical approaches. *Mol Phys*. 2007;*105*:2659–2666.
66. Quack M. Spectra and dynamics of coupled vibrations in polyatomic molecules. *Annu Rev Phys Chem*. 1990;*41*:839–874.
67. Halonen L. Local mode vibrations in polyatomic molecules. In: Prigogine I, Rice SA, editors. *Advances in Chemical Physics*. Volume 104. New York, NY: Wiley, 1998; p. 41–179.
68. Jensen P. An introduction to the theory of local mode vibrations. *Mol Phys*. 2000;*98*:1253–1285.
69. Jensen P. Local modes in vibration–rotation spectroscopy. *WIREs Comput Mol Sci*. 2012;*2*:494–512.
70. Albert S, Albert KK, Hollenstein H, Tanner CM, Quack M. Fundamentals of rotation-vibration spectra. In: Quack M, Merkt F, editors. *Handbook of High-resolution Spectroscopy*. Volume 3. New York, NY: Wiley, 2011; p. 117–173.
71. Ozaki Y, Huck CW, Ishigaki M, Ishikawa D, Shinzawa H. Near-infrared spectroscopy in biological molecules and tissues. In: Roberts G, Watts A, editors. *Encyclopedia of Biophysics*. Berlin, Heidelberg: Springer Berlin Heidelberg, 2018; p. 1–19.
72. Gerber RB, Chaban GM, Brauer B, Miller Y. First principles calculations of anharmonic vibrational spectroscopy of large molecules. In: Dykstra CE, Kim KS, Fleming G, Scuseria GE, editors. *Theory and Applications of Computational Chemistry: The First 40 Years*. Amsterdam, Netherlands: Elsevier Publications, 2005; p. 165–193.
73. Bowman JM, Carrington T, Meyer HD. Variational quantum approaches for computing vibrational energies of polyatomic molecules. *Mol Phys*. 2008;*106*:16–18.
74. Hansen MB, Sparta M, Seidler P, Toffoli D, Christiansen O. New formulation and implementation of vibrational self-consistent field theory. *J Chem Theory Comput*. 2010;*6*:235–248.
75. Piccardo M, Bloino J, Barone V. Generalized vibrational perturbation theory for rotovibrational energies of linear, symmetric and asymmetric tops: theory, approximations, and automated approaches to deal with medium-to-large molecular systems. *Int J Quant Chem*. 2015;*115*:948–982.
76. Egidi F, Williams-Young DB, Baiardi A, et al. Effective inclusion of mechanical and electrical anharmonicity in excited electronic states: VPT2-TDDFT route. *J Chem Theory Comput*. 2017;*13*:2789–2803.
77. Wang S. Efficiently calculating anharmonic frequencies of molecular vibration by molecular dynamics trajectory analysis. *ACS Omega*. 2019;*4*:9271–9283.
78. Wu J, Sousa C, de Graaf C. The role of vibrational anharmonicity in the computational study of thermal spin crossover. *Magnetochemistry*. 2019;5:49-1–49-14.
79. Latouche C, Palazzetti F, Skouteris D, Barone V. High-accuracy vibrational computations for transition-metal complexes including anharmonic corrections: ferrocene, ruthenocene, and osmocene as test cases. *J Chem Theory Comput*. 2014;*10*:4565–4573.
80. Yagi K, Yamada K, Kobayashi C, Sugita Y. Anharmonic vibrational analysis of biomolecules and solvated molecules using hybrid QM/-MM computations. *J Chem Theory Comput*. 2019;*15*:1924–1938.
81. Roy TK, Gerber RB. Vibrational self-consistent field calculations for spectroscopy of biological molecules: New algorithmic developments and applications. *Phys Chem Chem Phys*. 2013;*15*:9468–9492.
82. Wilson EB Jr. A method of obtaining the expanded secular equation for the vibration frequencies of a molecule. *J Chem Phys*. 1939;*7*: 1047–1052.
83. El'yashevich M. ComptRend. *Acad Sci URSS*. 1940;*28*:605.
84. Andrews DH. The relation between the Raman spectra and the structure of organic molecules. *Phys Rev*. 1930;*36*:544–554.
85. Dennison DM. The infrared spectra of polyatomic molecules. *Rev Mod Phys*. 1931;*3*:280–345.
86. Dennison DM. The infrared spectra of polyatomic molecules. Part II. *Rev Mod Phys*. 1940;*12*:175–214.
87. Linnett JW, Thompson H. Force constants and structure. *Nature*. 1937;*139*:509–510.
88. Linnett JW. Force constants. *Q Rev Chem Soc*. 1947;*1*:73–90.
89. Urey HC, Bradley CA Jr. The vibrations of pentatonic tetrahedral molecules. *Phys Rev*. 1931;*38*:1969–1978.
90. Hill TH. On steric effects. *J Chem Phys*. 1946;*15*:465–466.
91. Dostrovsky I, Hughes ED, Ingold CK. Mechanism of substitution at a saturated carbon atom. Part XXXII. The role of steric hindrance. (section G) magnitude of steric effects, range of occurrence of steric and polar effects, and place of the Wagner rearrangement in nucleophilic substitution and elimination. *J Chem Soc*. 1946;173–194.
92. Gordy W. A relation between bond force constants, bond orders, bond lengths, and the electronegativities of the bonded atoms. *J Chem Phys*. 1946;*14*:305–320.
93. Westheimer FH, Mayer JE. The theory of the racemization of optically active derivatives of diphenyl. *J Chem Phys*. 1946;*14*:733–738.
94. Westheimer FH. A calculation of the energy of activation for the racemization of 2,2′-dibromo-4,4′-dicarboxydiphenyl. *J Chem Phys*. 1947;*15*:252–260.
95. Allinger L. *U B. ACS Monograph 177: Molecular Mechanics*. Washington, DC: American Chemical Society, 1982.
96. Bowen J, Allinger N. Molecular mechanics: the art and science of parameterization. In: Lipkowitz KB, editor. *Reviews in Computational Chemistry*. Volume 2. New York, NY: VCH Publishers, 1991; p. 81–95.
97. Machida K. *Principles of Molecular Mechanics*. New York, NY: Wiley, 1999.

98. Decius J. Classical limit of mean thermal vibration amplitudes. *J Chem Phys*. 1953;*21*:1121–1122.
99. Cyvin SJ, Slater NB. Unvariance of molecular inverse force constants. *Nature*. 1960;*188*:485.
100. Decius J. Compliance matrix and molecular vibrations. *J Chem Phys*. 1963;*38*:241–248.
101. Jones LH, Swanson BI. Interpretation of potential constants: Application to study of bonding forces in metal cyanide complexes and metal carbonyls. *Acc Chem Res*. 1976;*9*:128–134.
102. Pople JA, Krishnan R, Schlegel HB, Binkley JS. Derivative studies in Hartree–Fock and Møller–Plesset theories. *Int J Quan Chem*. 1979;*16*(S13):225–241.
103. Gerratt J, Mills IM. Force constants and dipole-moment derivatives of molecules from perturbed Hartree–Fock calculations. *J Chem Phys*. 1968;*49*:1719–1729.
104. Pulay P. Second and third derivatives of variational energy expressions: application to multiconfigurational self-consistent field wave functions. *J Chem Phys*. 1983;*78*:5043–5051.
105. Fogarasi G, Pulay P. AB initio vibrational force fields. *Annu Rev Phys Chem*. 1984;*35*:191–213.
106. Forgarasi G, Pulay P. Ab initio calculations of force fields and vibrational spectra. In: Durig JR, editor. *Vibrational Spectra and Structure*. Volume 14. Amsterdam, Netherlands: Elsevier, 1985; p. 125–219.
107. Saxe P, Yamaguchi Y, Schaefer HF. Analytic second derivatives in restricted Hartree–Fock theory. A method for high-spin open-shell molecular wave functions. *J Chem Phys*. 1982;*77*(11):5647–5654.
108. Fox DJ, Osamura Y, Hoffmann MR, et al. Analytic energy second derivatives for general correlated wavefunctions, including a solution of the first-order coupled-perturbed configuration-interaction equations. *Chem Phys Lett*. 1983;*102*(1):17–19.
109. Schaefer HF, Yamaguchi Y. A new dimension to quantum chemistry: theoretical methods for the analytic evaluation of first, second, and third derivatives of the molecular electronic energy with respect to nuclear coordinates. *J Mol Struc THEOCHEM*. 1986;*135*: 369–390.
110. Koch H, Jensen HJA, Jørgensen P, Helgaker T, Scuseria GE, Schaefer HF. Coupled cluster energy derivatives. Analytic hessian for the closed-shell coupled cluster singles and doubles wave function: theory and applications. *J Chem Phys*. 1990;*92*(8):4924–4940.
111. Hoffmann MR, Fox DJ, Gaw JF, et al. Analytic energy second derivatives for general MCSCF wave functions. *J Chem Phys*. 1984;*80*(6): 2660–2668.
112. Handy NC, Schaefer HF. On the evaluation of analytic energy derivatives for correlated wave functions. *J Chem Phys*. 1984;*81*(11): 5031–5033.
113. Handy NC, Amos RD, Gaw JF, Rice JE, Simandiras ED. The elimination of singularities in derivative calculations. *Chem Phys Lett*. 1985;*120*(2):151–158.
114. Harrison RJ, Fitzgerald GB, Laidig WD, Barteltt RJ. Analytic MBPT(2) second derivatives. *Chem Phys Lett*. 1986;*124*(3):291–294.
115. Salter EA, Bartlett RJ. Analytic energy derivatives in many-body methods. II. Second derivatives. *J Chem Phys*. 1989;*90*(3):1767–1773.
116. Amos R, Rice J. Implementation of analytic derivative methods in quantum chemistry. *Comput Phys Rep*. 1989;*10*(4):147–187.
117. Helgacker T, Jørgensen P. Analytical calculation of geometrical derivatives in molecular electronic structure theory. *Adv Quantum Chem*. 1988;*19*:183–245.
118. Jørgensen P, Simons J. Ab initio analytical molecular gradients and hessians. *J Chem Phys*. 1983;*79*:1332.
119. Camp RN, King HF, McIver JW, Mullally D. Analytical force constants for MCSCF wave functions. *J Chem Phys*. 1983;*79*(2): 1088–1089.
120. Takada T, Dupuis M, King HF. Molecular symmetry. III. Second derivatives of electronic energy with respect to nuclear coordinates. *J Chem Phys*. 1981;*75*:1332.
121. Pulay P. Analytical derivatives, forces, force constants, molecular geometries, and related response properties in electronic structure theory. *WIREs Comput Mol Sci*. 2013;*4*(3):169–181.
122. Pulay P. *Analytical Derivative Methods in Quantum Chemistry*. New York, NY: John Wiley, 2007;p. 241–286.
123. Pulay P. Analytical derivative techniques and the calculation of vibrational spectra. *Modern Electronic Structure Theory*. Singapore: World Scientific Publishing Company, 1995; p. 1191–1240.
124. Amos RD. *Molecular Property Derivatives*. New York, NY: John Wiley, 2007;p. 99–153.
125. Yamaguchi Y, Schaefer HF III, Osamura Y, Goddard J. *A New Dimension to Quantum Chemistry: Analytical Derivative Methods in Ab Initio Molecular Electronic Structure Theory*. Oxford, England: Oxford University Press, 1994.
126. Stanton JF, Gauss J. Analytic second derivatives in high-order many-body perturbation and coupled-cluster theories: computational considerations and applications. *Int Rev Phys Chem*. 2000;*19*(1):61–95.
127. Bast R, UE m, Gao B, Helgaker T, Ruud K, Thorvaldsen AJ. The ab initio calculation of molecular electric, magnetic and geometric properties. *Phys Chem Chem Phys*. 2011;*13*:2627–2651.
128. Helgaker T, Coriani S, Jørgensen P, Kristensen K, Olsen J, Ruud K. Recent advances in wave function-based methods of molecular-property calculations. *Chem Rev*. 2012;*112*:543–631.
129. Brandhorst K, Grunenberg J. How strong is it? The interpretation of force and compliance constants as bond strength descriptors. *Chem Soc Rev*. 2008;*37*(8):1558–1567.
130. Brandhorst K, Grunenberg J. Efficient computation of compliance matrices in redundant internal coordinates from Cartesian hessians for nonstationary points. *J Chem Phys*. 2010;*132*:184101.
131. Grunenberg J. Ill-defined concepts in chemistry: rigid force constants vs. compliance constants as bond strength descriptors for the triple bond in diboryne. *Chem Sci*. 2015;*6*(7):4086–4088.

132. Kreft A, Lücht A, Grunenberg J, Jones PG, Werz DB. Kinetic studies of donor–acceptor cyclopropanes: the influence of structural and electronic properties on the reactivity. *Angew Chem Int Ed*. 2019;*58*(7):1955–1959.
133. Pandey SK, Manogaran D, Manogaran S, Schaefer HF. Quantification of hydrogen bond strength based on interaction coordinates: a new approach. *J Phys Chem A*. 2017;*121*(32):6090–6103.
134. Dash J, Ray S, Devi N, Basutkar N, Ambade AV, Pesala B. Fine-tuning of terahertz resonances in hydrogen-bonded organic molecular complexes. *J Mol Struct*. 2019;*1184*:495–502.
135. Madhav MV, Manogaran S. A relook at the compliance constants in redundant internal coordinates and some new insights. *J Chem Phys*. 2009;*131*:174112-1–1174112-6.
136. Vicharelli PA, McDonald FA. Generalized classical theory of intramolecular coordinate relaxation in polyatomic molecules. *J Chem Phys*. 1980;*72*(8):4627–4636.
137. Baker J, Pulay P. The interpretation of compliance constants and their suitability for characterizing hydrogen bonds and other weak interactions. *J Am Chem Soc*. 2006;*128*:11324–11325.
138. Baker J. Compliance constants: Are they of any real use? *WIREs Comput Mol Sci*. 2014;*4*:111–115.
139. McKean DC. Individual CH bond strengths in simple organic compounds: Effects of conformation and substitution. *Chem Soc Rev*. 1978;*7*:399.
140. Larsson JA, Cremer D. Theoretical verification and extension of the Mckean relationship between bond lengths and stretching frequencies. *J Mol Struct*. 1999;485–486:385–407.
141. Kittel C. *Introduction to Solid State Physics*. New York, NY: Wiley, 2005.
142. Turrell G. *Infrared and Raman Spectra of Crystals*. New York, NY: Academic Press, 1972.
143. Birman JL. *Theory of Crystal Space Groups and Lattice Dynamics: Infra-Red and Raman Optical Processes of Insulating Crystals*. Berlin Heidelberg: Springer, 2012.
144. Tuschel D. Raman spectroscopy and polymorphism. *Spectroscopy*. 2019;*34*:10–21.
145. Sokolov VI, Grudzev NB, Farina IA. Local vibrational mode in zinc telluride associated with a charged nickel impurity. *Phys Solid State*. 2003;*45*:1638–1643.
146. Sangster MJL, Harding JH. Calculation of local and gab mode frequencies from impurities in alkali halide crystals. *J Phys C Solid State Phys*. 1986;*19*:6153–6158.
147. Güngerich M, Sander T, Heiliger C, Czerner M, Klar PJ. Local N environment in the dilute nitrides Ga(N,P), Ga(N,As), and Ga(N,Sb). *Phys Status Solidi (b)*. 2013;*250*(4):755–759.
148. Sanson A, Napolitani E, Impellizzeri G, et al. Investigation of germanium implanted with aluminum by multi-laser micro-Raman spectroscopy. *Thin Solid Films*. 2013;*541*(4):76–78.
149. Sanson A, Giarola M, Napolitani E, et al. Study of carrier concentration profiles in Al-implanted Ge by micro-Raman spectroscopy under different excitation wavelengths. *J Raman Spectrosc*. 2013;*44*(5):665–669.
150. Markevich VP, Peaker AR, Hamilton B, et al. The trivacancy and trivacancy-oxygen family of defects in silicon. *Solid State Phenom*. 2014;*205*:181–190.
151. Parmar N, Mccluskey M, Lynn K. Vibrational spectroscopy of Na—H complexes in ZnO. *J Electron Mater*. 2013;*12*(42):3426–3428.
152. Jacob CR, Luber S, Reiher M. Understanding the signatures of secondary-structure elements in proteins with Raman optical activity spectroscopy. *Chem A Eur J*. 2009;*15*(48):13491–13508.
153. Jacob CR, Reiher M. Localizing normal modes in large molecules. *J Chem Phys*. 2009;*130*:084106.
154. Liegeois V, Jacob CR, Champagne B, Reiher M. Analysis of vibrational Raman optical activity signatures of the (TG)N and (GG)N conformations of isotactic polypropylene chains in terms of localized modes. *J Phys Chem A*. 2010;*114*:7198–7212.
155. Cheng X, Steele RP. Efficient anharmonic vibrational spectroscopy for large molecules using local-mode coordinates. *J Chem Phys*. 2014;*141*(10):104105.
156. Panek PT, Hoeske AA, Jacob CR. On the choice of coordinates in anharmonic theoretical vibrational spectroscopy: harmonic vs. anharmonic coupling in vibrational configuration interaction. *J Chem Phys*. 2019;*150*:054107-1–054107-23.
157. Cline D. *Variational Principles in Classical Mechanics*. Rochester, NY: University of Rochester River Campus Libraries, 2017.
158. Hsu CP. The electronic couplings in electron transfer and excitation energy transfer. *Acc Chem Res*. 2009;*42*:509–518.
159. Wang CI, Braza MKE, Claudio GC, Nellas RB, Hsu CP. Machine learning for predicting electron transfer coupling. *J Phys Chem A*. 2019;*123*:7792–7802.
160. Woodward LA. *Introduction to the Theory of Molecular Vibrations and Vibrational Spectroscopy*. Oxford, England: Oxford University Press, 1972.
161. Califano S. *Vibrational States*. New York, NY: Wiley, 1976.
162. Groner P. *Normal Coordinate Analysis*. New York, NY: John Wiley, 2006.
163. Kelley JD, Leventhal JJ. Normal modes and coordinates. *Problems in Classical and Quantum Mechanics*. Berlin, Germany: Springer, 2017; p. 95–117.
164. Neto N. Tensor formalism in anharmonic calculations. *Chem Phys*. 1984;*91*:89.
165. Stare J. First-principle calculation of reduced masses in vibrational analysis using generalized internal coordinates: some crucial aspects and examples. *J Chem Inf Model*. 2007;*47*(3):840–850.
166. Zou W, Kalescky R, Kraka E, Cremer D. Relating normal vibrational modes to local vibrational modes with the help of an adiabatic connection scheme. *J Chem Phys*. 2012;*137*:084114.

167. Zou W, Cremer D. C_2 in a box: determining its intrinsic bond strength for the $X^1\Sigma_g^+$ ground state. *Chem A Eur J*. 2016;*22*:4087–4097.
168. Cremer D, Kraka E. From molecular vibrations to bonding, chemical reactions, and reaction mechanism. *Curr Org Chem*. 2010;*14*: 1524–1560.
169. Kalescky R, Kraka E, Cremer D. Identification of the strongest bonds in chemistry. *J Phys Chem A*. 2013;*117*:8981–8995.
170. Mayer I. Charge, bond order and valence in the ab initio theory. *Chem Phys Lett*. 1983;*97*:270–274.
171. Mayer I. Bond orders and valences from ab initio wave functions. *Int J Quantum Chem*. 1986;*29*:477–483.
172. Mayer I. Bond order and valence indices: a personal account. *J Comput Chem*. 2007;*28*(1):204–221.
173. Zou W, Cremer D. Properties of local vibrational modes: The infrared intensity. *Theor Chem Acc*. 2014;*133*:1451–1466.
174. Kalescky R, Zou W, Kraka E, Cremer D. Local vibrational modes of the water dimer—comparison of theory and experiment. *Chem Phys Lett*. 2012;*554*:243–247.
175. Kalescky R, Kraka E, Cremer D. Local vibrational modes of the formic acid dimer - the strength of the double H-bond. *Mol Phys*. 2013; *111*:1497–1510.
176. Johnson R. *NIST Computational Chemistry Comparison and Benchmark Database—NIST Standard Reference Database Number 101*. National Institute of Standards and Technology; 2019. http://cccbdb.nist.gov/
177. Bak O, Borowski P. Scaling procedures in vibrational spectroscopy. In: Koleżyński A, Król M, editors. *Molecular Spectroscopy-Experiment and Theory: From Molecules to Functional Materials*. New York, NY: Springer, 2019; p. 49–95.
178. Kesharwani MK, Brauer B, MJM L. Frequency and zero-point vibrational energy scale factors for double-hybrid density Functionals (and other selected methods): Can anharmonic force fields be avoided? *J Chem Phys*. 2015;*119*:1701–1714.
179. Witek HA, Morokuma K. Systematic study of vibrational frequencies calculated with the self-consistent charge density functional tight-binding method. *Int J Quant Chem*. 2004;*25*:1858–1864.
180. Mizugai Y, Katayama M. The 5th overtone of the C—H stretching vibrations and the bond lengths in some heterocyclic-compounds. *Chem Phys Lett*. 1980;*73*:240–243.
181. Wong JS, Moore CB. Inequivalent C—H oscillators of gaseous alkanes and alkenes in laser photo-acoustic overtone spectroscopy. *J Chem Phys*. 1982;*77*:603–615.
182. Sbrana G, Muniz-Miranda M. High overtones of c-h stretching vibrations in isoxazole, thiazole, and related methyl and dimethyl derivatives. *J PhysChem A*. 1998;*102*:7603–7608.
183. Hippler M, Quack M. Intramolecular energy transfer from isotope selective overtone spectroscopy by vibrationally assisted dissociation and photo-fragment ionization. *Ber Bunsen Phys Chem*. 1997;*101*:356–362.
184. Hollensteun H, Luckhaus D, Quack M. Dynamics of the CH chromophore in CH_{x3}—a combined treatment for a set of isotopic-species. *J Mol Struct*. 1993;*294*:65–70.
185. Chai JD, Head-Gordon M. Long-range corrected hybrid density functionals with damped atom-atom dispersion corrections. *Phys Chem Chem Phys*. 2008;*10*:6615–6620.
186. Dunning TH. Gaussian basis sets for use in correlated molecular calculations. I. The atoms boron through neon and hydrogen. *J Chem Phys*. 1989;*90*(2):1007–1023.
187. Kendall RA, Dunning TH, Harrison RJ. Electron affinities of the first-row atoms revisited. Systematic basis sets and wave functions. *J Chem Phys*. 1992;*96*(9):6796–6806.
188. Stark J. Observation of the separation of spectral lines by an electric field. *Nature*. 1913;*92*:401–401.
189. Chattopadhyay A, Boxer SG. Vibrational stark effect spectroscopy. *J Am Chem Soc*. 1995;*117*:1449–1450.
190. Bublitz GU, Boxer SG. Stark spectroscopy: Applications in chemistry, biology, and materials science. *Annu Rev Phys Chem*. 1997;*48*:213–242.
191. Boxer SG. Stark realities. *J Phys Chem B*. 2009;*113*(10):2972–2983.
192. Fried SD, Boxer SG. Measuring electric fields and noncovalent interactions using the vibrational Stark effect. *Acc Chem Res*. 2015;*48*: 998–1006.
193. Ma J, Pazos IM, Zhang W, Culik RM, Gai F. Site-specific infrared probes of proteins. *Annu Rev Phys Chem*. 2015;*66*(1):357–377.
194. Fried SD, Boxer SG. Electric fields and enzyme catalysis. *Annu Rev Biochem*. 2017;*86*:387–415.
195. Adhikary R, Zimmermann J, Romesberg FE. Transparent window vibrational probes for the characterization of proteins with high structural and temporal resolution. *Chem Rev*. 2017;*117*(3):1927–1969.
196. Błasiak B, Londergan CH, Webb LJ, Cho M. Vibrational probes: From small molecule solvatochromism theory and experiments to applications in complex systems. *Acc Chem Res*. 2017;*50*(4):968–976.
197. Slocum JD, Webb LJ. Measuring electric fields in biological matter using the vibrational stark effect of nitrile probes. *Annu Rev Phys Chem*. 2018;*69*:253–271.
198. Welborn VV, Head-Gordon T. Computational design of synthetic enzymes. *Chem Rev*. 2018;*119*(11):6613–6630.
199. Thiel W, Hummer G. Methods for computational chemistry. *Nature*. 2013;*504*(7478):96–97.
200. Barnes L, Schindler B, Compagnon I, Allouche AR. Fast and accurate hybrid QM/MM approach for computing anharmonic corrections to vibrational frequencies. *J Mol Model*. 2016;*22*(11):285-1–285-13.
201. Senn HM, Thiel W. QM/MM methods for biomolecular systems. *Angew Chem Int Ed*. 2009;*48*(7):1198–1229.
202. Vreven T, Morokuma K. Hybrid methods: ONIOM(QM:MM) and QM/MM. *Annual Reports in Computational Chemistry*. Amsterdam, Netherlands: Elsevier, 2006; p. 35–51.
203. Gao J. Hybrid quantum and molecular mechanical simulations:? An alternative avenue to solvent effects in organic chemistry. *Acc Chem Res*. 1996;*29*:298–305.

204. Head JD. Computation of vibrational frequencies for adsorbates on surfaces. *Int J Quantum Chem*. 1997;*65*(5):827–838.
205. Li H, Jensen JH. Partial hessian vibrational analysis: The localization of the molecular vibrational energy and entropy. *Theor Chem Acc*. 2002;*107*(4):211–219.
206. Ghysels A, Van Neck D, Van Speybroeck V, Verstraelen T, Waroquier M. Vibrational modes in partially optimized molecular systems. *J Chem Phys*. 2007;*126*(22):224102.
207. Ghysels A, Van Neck D, Waroquier M. Cartesian formulation of the mobile block Hessian approach to vibrational analysis in partially optimized systems. *J Chem Phys*. 2007;*127*(16):164108.
208. Ghysels A, Van Neck D, Brooks BR, Van Speybroeck V, Waroquier M. Normal modes for large molecules with arbitrary link constraints in the Mobile block Hessian approach. *J Chem Phys*. 2009;*130*(8):084107.
209. Ghysels A, Van Speybroeck V, Pauwels E, Van Neck D, Brooks BR, Waroquier M. Mobile block Hessian approach with adjoined blocks: An efficient approach for the calculation of frequencies in macromolecules. *J Chem Theory Comput*. 2009;*5*(5):1203–1215.
210. Woodcock HL, Zheng W, Ghysels A, Shao Y, Kong J, Brooks BR. Vibrational subsystem analysis: A method for probing free energies and correlations in the harmonic limit. *J Chem Phys*. 2008;*129*(21):214109-1–214109-19.
211. Ghysels A, Van Speybroeck V, Pauwels E, et al. Comparative study of various normal mode analysis techniques based on partial hessians. *J Comput Chem*. 2010;*31*(5):994–1007.
212. Huix-Rotllant M, Ferré N. An effective procedure for analyzing molecular vibrations in terms of local fragment modes. *J Chem Theory Comput*. 2016;*12*(10):4768–4777.
213. Tao Y, Tian C, Verma N, et al. Recovering intrinsic fragmental vibrations using the generalized subsystem vibrational analysis. *J Chem Theory Comput*. 2018;*14*:2558–2569.
214. Campbell SL, Meyer CD. *Generalized Inverses of Linear Transformations*. London, England: Society for Industrial and Applied Mathematics, 2008.
215. Penrose R. Generalized inverse for matrices. *Proc Cambridge Phil Soc*. 1955;*51*:406–413.
216. Becke AD. Density-functional thermochemistry. III. The role of exact exchange. *J Chem Phys*. 1993 apr;*98*(7):5648–5652.
217. Lee C, Yang W, Parr RG. Development of the Colle–Salvetti correlation-energy formula into a functional of the electron density. *Phys Rev B*. 1988;*37*(2):785–789.
218. Vosko SH, Wilk L, Nusair M. Accurate spin-dependent electron liquid correlation energies for local spin density calculations: A critical analysis. *Can J Phys*. 1980 aug;*58*(8):1200–1211.
219. Stephens PJ, Devlin FJ, Chabalowski CF, Frisch MJ. Ab initio calculation of vibrational absorption and circular dichroism spectra using density functional force fields. *J Phys Chem*. 1994 nov;*98*(45):11623–11627.
220. Grimme S, Antony J, Ehrlich S, Krieg H. A consistent and accurate *ab initio* parametrization of density functional dispersion correction (DFT-D) for the 94 elements H-Pu. *J Chem Phys*. 2010;*132*(15):154104.
221. Grimme S, Ehrlich S, Goerigk L. Effect of the damping function in dispersion corrected density functional theory. *J Comput Chem*. 2011;*32*(7):1456–1465.
222. Krishnan R, Binkley JS, Seeger R, Pople JA. Self-consistent molecular orbital methods. XX. A basis set for correlated wave functions. *J Chem Phys*. 1980;*72*:650–654.
223. Tao Y, Zou W, Sethio D, et al. In situ measure of intrinsic bond strength in crystalline structures: Local vibrational mode theory for periodic systems. *J Chem Theory Comput*. 2019;*15*:1761–1776.
224. Born M, Huang K. *Dynamical Theory of Crystal Lattices*. Oxford, England: Clarendon Press, 1954.
225. Dovesi R, Erba A, Orlando R, et al. Quantum-mechanical condensed matter simulations with CRYSTAL. *WIREs Comput Mol Sci*. 2018;*8*(4):e1360.
226. Pascale F, Zicovich-Wilson CM, Gejo FL, Civalleri B, Orlando R, Dovesi R. The calculation of the vibrational frequencies of crystalline compounds and its implementation in the CRYSTAL code. *J Comput Chem*. 2004 mar;*25*(6):888–897.
227. Civalleri B, Pascale F, Noel Y. Vibrational frequencies calculation. *CRYSTAL*. 2017;*2017*.
228. Gamboa A, Vignoles GL, Leyssale JM. On the prediction of graphene's elastic properties with reactive empirical bond order potentials. *Carbon*. 2015;*89*:176–187.
229. Allen MJ, Tung VC, Kaner RB. Honeycomb carbon: A review of graphene. *Chem Rev*. 2010;*110*:132–145.
230. Ghuge AD, Shirode AR, Kadam VJ. Graphene: A comprehensive review. *Curr Drug Targets*. 2017 mar;*18*(6):724–733.
231. Choi W, Lahiri I, Seelaboyina R, Kang YS. Synthesis of graphene and its applications: A review. *Crit Rev Solid State*. 2010 feb;*35*(1):52–71.
232. Neto AHC, Guinea F, Peres NMR, Novoselov KS, Geim AK. The electronic properties of graphene. *Rev Mod Phys*. 2009 jan;*81*(1):109–162.
233. Pierson HO. *Handbook of Carbon, Graphite, Diamonds and Fullerenes: Processing, Properties and Applications (Materials Science and Process Technology)*. Park Ridge, NJ: Noyes Publications, 2012.
234. Hom T, Kiszenik W, Post B. Accurate lattice constants from multiple reflection measurements. II. Lattice constants of germanium silicon, and diamond. *J Appl Cryst*. 1975;*8*:457–458.
235. Luo YR. *Comprehensive Handbook of Chemical Bond Energies*. Boca Raton, FL: CRC Press, 2007.
236. Earl JC. Carbon–carbon bond energies. *Tetrahedron*. 1960;*9*:65–66.
237. Popov IV, Görne AL, Tchougreeff AL, Dronskowski R. Relative stability of diamond and graphite as seen through bonds and hybridizations. *PhysChemChemPhys*. 2019;*21*:10961–10969.

238. Hu M, He J, Zhao Z, et al. Compressed glassy carbon: an ultrastrong and elastic interpenetrating graphene network. *Sci Adv*. 2017;*3*: e1603213-1–e1603213-7.
239. Yuan Q, Lin CT, Chee KWA. All-carbon devices based on sp^2-on-sp^3 configuration. *APL Mater*. 2019;*7*:030901-1–030901-7.
240. Tasis D, Tagmatarchis N, Bianco A, Prato M. Chemistry of carbon nanotubes. *Chem Rev*. 2006 mar;*106*(3):1105–1136.
241. Setiawan D, Sethio D, Cremer D, Kraka E. From strong to weak NF bonds: on the design of a new class of fluorinating agents. *Phys Chem Chem Phys*. 2018;*20*:23913–23927.
242. Humason A, Zou W, Cremer D. 11,11-Dimethyl-1,6-methano[10]annulene-an annulene with an ultralong CC bond or a fluxional molecule? *J Phys Chem A*. 2014;*119*:1666–1682.
243. Kalescky R, Kraka E, Cremer D. Are carbon-halogen double and triple bonds possible? *Int J Quant Chem*. 2014;*114*:1060–1072.
244. Kalescky R, Zou W, Kraka E, Cremer D. Quantitative assessment of the multiplicity of carbon-halogen bonds: carbenium and halonium ions with F, Cl, Br, and I. *J Phys Chem A*. 2014;*118*:1948–1963.
245. Cremer D, Wu A, Larsson JA, Kraka E. Some thoughts about bond energies, bond lengths, and force constants. *J Mol Model*. 2000;*6*: 396–412.
246. Kraka E, Cremer D. Weaker bonds with shorter bond lengths. *Rev Proc Quim*. 2012;*6*(11):31–34.
247. Setiawan D, Kraka E, Cremer D. Hidden bond anomalies: The peculiar case of the fluorinated amine chalcogenides. *J Phys Chem A*. 2015;*119*:9541–9556.
248. Kraka E, Setiawan D, Cremer D. Re-evaluation of the bond length-bond strength rule: the stronger bond is not always the shorter bond. *J Comput Chem*. 2015;*37*:130–142.
249. Freindorf M, Kraka E, Cremer D. A comprehensive analysis of hydrogen bond interactions based on local vibrational modes. *Int J Quant Chem*. 2012;*112*:3174–3187.
250. Kalescky R, Zou W, Kraka E, Cremer D. Vibrational properties of the isotopomers of the water dimer derived from experiment and computations. *Aust J Chem*. 2014;*67*:426.
251. Tao Y, Zou W, Jia J, Li W, Cremer D. Different ways of hydrogen bonding in water—why does warm water freeze faster than cold water? *J Chem Theory Comput*. 2017;*13*:55–76.
252. Tao Y, Zou W, Kraka E. Strengthening of hydrogen bonding with the push-pull effect. *Chem Phys Lett*. 2017;*685*:251–258.
253. Freindorf M, Tao Y, Sethio D, Cremer D, Kraka E. New mechanistic insights into the Claisen rearrangement of chorismate—a unified reaction valley approach study. *Mol Phys*. 2018;*117*:1172–1192.
254. Makoś MZ, Freindorf M, Sethio D, Kraka E. New insights into Fe−H_2 and Fe−H^- bonding of a [NiFe] hydrogenase mimic—a local vibrational mode study. *Theor Chem Acc*. 2019;*138*:76–1–76–18.
255. Lyu S, Beiranvand N, Freindorf M, Kraka E. Interplay of ring puckering and hydrogen bonding in deoxyribonucleosides. *J Phys Chem A*. 2019;*123*:7087–7103.
256. Oliveira V, Kraka E, Cremer D. The intrinsic strength of the halogen bond: electrostatic and covalent contributions described by coupled cluster theory. *Phys Chem Chem Phys*. 2016;*18*:33031–33046.
257. Oliveira V, Kraka E, Cremer D. Quantitative assessment of halogen bonding utilizing vibrational spectroscopy. *Inorg Chem*. 2016;*56*: 488–502.
258. Oliveira V, Cremer D. Transition from metal-ligand bonding to halogen bonding involving a metal as halogen acceptor: a study of Cu, Ag, Au, Pt, and Hg complexes. *Chem Phys Lett*. 2017;*681*:56–63.
259. Yannacone S, Oliveira V, Verma N, Kraka E. A continuum from halogen bonds to covalent bonds: Where do λ^3 Iodanes fit? *Inorganics*. 2019;*7*(47):1–23.
260. Oliveira VP, Kraka E, Machado FBC. Pushing 3c-4e bonds to the limit: A coupled cluster study of stepwise fluorination of first-row atoms. *Inorg Chem*. 2019;*58*:14777–14789.
261. Oliveira VP, Marcial BL, Machado FBC, Kraka E. Metal-halogen bonding seen through the eyes of vibrational spectroscopy. *Materials*. 2020;*13*:55–1–55–23.
262. Setiawan D, Kraka E, Cremer D. Description of Pnicogen bonding with the help of vibrational spectroscopy-the missing link between theory and experiment. *Chem Phys Lett*. 2014;*614*:136–142.
263. Setiawan D, Kraka E, Cremer D. Strength of the Pnicogen bond in complexes involving group VA elements N, P, and As. *J Phys Chem A*. 2014;*119*:1642–1656.
264. Setiawan D, Cremer D. Super-Pnicogen bonding in the radical anion of the fluorophosphine dimer. *Chem Phys Lett*. 2016;*662*:182–187.
265. Oliveira V, Cremer D, Kraka E. The many facets of chalcogen bonding: described by vibrational spectroscopy. *J Phys Chem A*. 2017; *121*:6845–6862.
266. Oliveira V, Kraka E. Systematic coupled cluster study of noncovalent interactions involving halogens, chalcogens, and pnicogens. *J Phys Chem A*. 2017;*121*:9544–9556.
267. Sethio D, Oliveira V, Kraka E. Quantitative assessment of tetrel bonding utilizing vibrational spectroscopy. *Molecules*. 2018;*23*:2763.
268. Zhang X, Dai H, Yan H, Zou W, Cremer D. B—H π interaction: a new type of nonclassical hydrogen bonding. *J Am Chem Soc*. 2016; *138*:4334–4337.
269. Zou W, Zhang X, Dai H, Yan H, Cremer D, Kraka E. Description of an unusual hydrogen bond between carborane and a phenyl group. *J Org Chem*. 2018;*856*:114–127.
270. Setiawan D, Kraka E, Cremer D. Quantitative assessment of aromaticity and antiaromaticity utilizing vibrational spectroscopy. *J Org Chem*. 2016;*81*:9669–9686.

271. Li Y, Oliveira V, Tang C, Cremer D, Liu CG, Ma J. The peculiar role of the Au_3 unit in Au_m clusters: σ-aromaticity of the Au_5Zn^+ ion. *Inorg Chem*. 2017;*56*:5793–5803.
272. Kalescky R, Kraka E, Cremer D. Description of aromaticity with the help of vibrational spectroscopy: Anthracene and phenanthrene. *J Phys Chem A*. 2013;*118*:223–237.
273. Kalescky R, Kraka E, Cremer D. New approach to Tolman's electronic parameter based on local vibrational modes. *Inorg Chem*. 2013; *53*:478–495.
274. Setiawan D, Kalescky R, Kraka E, Cremer D. Direct measure of metal-ligand bonding replacing the Tolman electronic parameter. *Inorg Chem*. 2016;*55*:2332–2344.
275. Cremer D, Kraka E. Generalization of the Tolman electronic parameter: the metal–ligand electronic parameter and the intrinsic strength of the metal-ligand bond. *Dalton Trans*. 2017;*46*:8323–8338.
276. Li Y, Liu C, Oliveira V, Cremer D, Chen Z, Ma J. Odd-even effect of the number of free valence electrons on the electronic structure properties of gold-thiolate clusters. *Mol Phys*. 2018;*117*:1442–1450.
277. Tao Y, Zou W, Cremer D, Kraka E. Characterizing chemical similarity with vibrational spectroscopy: New insights into the substituent effects in Monosubstituted benzenes. *J Phys Chem A*. 2017;*121*:8086–8096.
278. Tao Y, Zou W, Cremer D, Kraka E. Correlating the vibrational spectra of structurally related molecules: a spectroscopic measure of similarity. *J Comput Chem*. 2017;*39*:293–306.
279. Verma N, Tao Y, Marcial BL, Kraka E. Correlation between molecular acidity (pka) and vibrational spectroscopy. *J Mol Model*. 2019; *25*:48.
280. Kraka E, Freindorf M, Cremer D. Chiral discrimination by vibrational spectroscopy utilizing local modes. *Chirality*. 2013;*25*:185–196.
281. Kraka E. Reaction path Hamiltonian and the unified reaction valley approach. *WIREs Comput Mol Sci*. 2011;*1*:531–556.
282. Kraka E, Zou W, Freindorf M, Cremer D. Energetics and mechanism of the hydrogenation of XH_n for group IV to group VII elements X. *J Chem Theory Comput*. 2012;*8*:4931–4943.
283. Kraka E, Cremer D. Dieter Cremer's contribution to the field of theoretical chemistry. *Int J Quantum Chem*. 2019;*119*:e25849.
284. Konkoli Z, Kraka E, Cremer D. Unified Reaction Valley approach mechanism of the reaction $CH_3 + H_2 \rightarrow CH_4 + H$. *J Phys Chem A*. 1997;*101*:1742–1757.
285. Cremer D, Wu A, Kraka E. The mechanism of the reaction $FH + H_2C = CH_2 \rightarrow H_2C{-}CFH_3$. Investigation of hidden intermediates with the unified reaction valley approach. *Phys Chem Chem Phys*. 2001;*3*:674–687.
286. Freindorf M, Sexton T, Kraka E, Cremer D. The mechanism of the cycloaddition reaction of 1,3-dipole molecules with acetylene - an investigation with the unified reaction valley approach. *Theor Chem Acc*. 2013;*133*:1423–1441.
287. Zou W, Sexton T, Kraka E, Freindorf M, Cremer D. A new method for describing the mechanism of a chemical reaction based on the unified reaction valley approach. *J Chem Theory Comput*. 2016;*12*:650–663.
288. Zou W, Tao Y, Freindorf M, Cremer D, Kraka E. Local vibrational force constants - from the assessment of empirical force constants to the description of bonding in large systems. *Chem Phys Lett*. 2020;*748*:137337.
289. Tao Y, Qiu Y, Zou W, Nanayakkara S, Yannacone S, Kraka E. In situ assessment of intrinsic strength of X─I···OA type halogen bonds in molecular crystals with periodic local vibrational mode theory. *Molecules*. 2020;*25*:1589.
290. Shaik S, Rzepa HS, Hoffmann R. One molecule, two atoms, three views, four bonds? *Angew Chem Int Ed Engl*. 2013;*52*:3020–3033.
291. Xu LT, Dunning TH. Insights into the perplexing nature of the bonding in C_2 from generalized valence bond calculations. *J Chem Theory Comput*. 2014;*10*:195–201.
292. Cooper DL, Penotti FE, Ponecc R. Why is the bond multiplicity in C_2 so illusive? *Comp Theor Chem*. 2015;*1053*:189–194.
293. Hermann M, Frenking G. The chemical bond in C_2. *Chem A Eur J*. 2016;*22*:44100–44108.
294. Kraka E, Cremer D. Chemical implication of local features of the electron density distribution. In: Maksic ZB, editor. *Theoretical Models of Chemical Bonding. The Concept of the Chemical Bond*. Volume 2. Verlag, Heidelberg: Springer, 1990; p. 453.
295. Kraka E, Cremer D. Description of chemical reactions in terms of the properties of the electron density. *J Mol Struct (THEOCHEM)*. 1992;*255*:189–206.
296. Clar E. *The Aromatic Sextet*. New York, NY: John Wiley & Sons, 1972.
297. Mpemba EB, Osborne DG. Cool? *Phys Education*. 1969;*4*:172–175.
298. Kemsley J. Why warm water freezes faster than cold water. *Chem Eng News*. 2017;*95*:8.
299. Tolman CA. Phosphorus ligand exchange equilibriums on zerovalent nickel. Dominant role for steric effects. *J Am Chem Soc*. 1970;*92* (10):2953–2956.
300. Tolman CA. The 16 and 18 electron rule in organometallic chemistry and homogeneous catalysis. *Chem Soc Rev*. 1972;*1*(3):337.
301. Tolman CA. Steric effects of phosphorus ligands in organometallic chemistry and homogeneous catalysis. *Chem Rev*. 1977;*77*:313–348.
302. Perrin L, Clot E, Eisenstein O, Loch J, Crabtree RH. Computed ligand electronic parameters from quantum chemistry and their relation to Tolman parameters, lever parameters, and Hammett constants. *Inorg Chem*. 2001;*40*:5806–5811.
303. Gusev DG. Donor properties of a series of two-electron ligands. *Organometallics*. 2009;*28*(3):763–770.
304. Zobi F. Ligand electronic parameters as a measure of the polarization of the C═O bond in $[M(CO)_xL_y]^n$ complexes and of the relative stabilization of $[M(CO)_xL_y]^{n/n+1}$ species. *Inorg Chem*. 2010;*49*(22):10370–10377.
305. Durand DJ, Fey N. Computational ligand descriptors for catalyst design. *Chem Rev*. 2019;*119*(11):6561–6594.
306. Fey N, Orpen AG, Harvey JN. Building ligand knowledge bases for organometallic chemistry computational description of phosphorus(III)-donor ligands and the metal–phosphorus bond. *Coord Chem Rev*. 2009;*253*(5–6):704–722.

307. Fey N. The contribution of computational studies to organometallic catalysis descriptors, mechanisms and models. *Dalton Trans*. 2010; *39*:296–310.
308. Kühl O. Predicting the net donating ability of phosphines—do we need sophisticated theoretical methods? *Coord Chem Rev*. 2005;*249*: 693–704.
309. McIntosh AI, Yang B, Goldup SM, Watkinson M, Donnan RS. Terahertz spectroscopy: a powerful new tool for the chemical sciences? *Chem Soc Rev*. 2012;*41*:2072–2082.
310. Mantsch HH, Naumann D. Terahertz spectroscopy: The renaissance of far infrared spectroscopy. *J Mol Struct*. 2010;*964*:1–4.
311. Parrott EPJ, Sun Y, Pickwell-MacPherson E. Terahertz spectroscopy: Its future role in medical diagnoses. *J Mol Struct*. 2011;*1006*: 66–76.
312. Körsgen H, Urban W, Brown JM. The infrared spectrum of FeH_2, studied in the gas phase by laser magnetic resonance. *J Chem Phys*. 1999;*110*(8):3861–3869.
313. Carroll PK, McCormack P. The spectrum of FeH: laboratory and solar identification. *Astrophys J*. 1972;*177*:L33.
314. DeYonker NJ, Allen WD. Taming the low-lying electronic states of FeH. *J Chem Phys*. 2012;*137*(23):234303.
315. Li HW, Zhu M, Buckley C, Jensen T. Functional materials based on metal hydrides. *Inorganic*. 2018;*6*(3):91.
316. Nakazawa H, Itazaki M. Fe −H complexes in catalysis. In: Plietker B, editor. *Iron Catalysis: Fundamentals and Applications*. Berlin, Heidelberg: Springer, Berlin Heidelberg, 2011; p. 27–81.
317. Glendening ED, Landis CR, Weinhold F. NBO 6.0: Natural bond orbital analysis program. *J Comput Chem*. 2013;*34*(16):1429–1437.
318. Reed AE, Weinstock RB, Weinhold F. Natural population analysis. *J Chem Phys*. 1985;*83*(2):735–746.
319. Zou W, Izotov D, Cremer D. New way of describing static and dynamic deformations of the Jahn–Teller type in ring molecules. *J Phys Chem A*. 2011;*115*:8731–8742.
320. Zou W, Filatov M, Cremer D. Bond pseudorotation, Jahn–Teller, and Pseudo–Jahn–Teller effects in the cyclopentadienyl cation and its pentahalogeno derivatives. *Int J Quant Chem*. 2012;*112*:3277–3288.
321. Zou W, Cremer D. Description of bond pseudorotation, bond pseudolibration, and ring pseudoinversion processes caused by the Pseudo–Jahn–Teller effect: Fluoro derivatives of the cyclopropane radical cation. *Aust J Chem*. 2014;*67*:435.
322. Jahn MK, Dewald DA, López MV, et al. Pseudorotational landscape of seven-membered rings: the most stable chair and twist-boat conformers of ϵ-caprolactone. *Chem A Eur J*. 2014;*20*:14084–14089.
323. Cremer D, Pople JA. General definition of ring puckering coordinates. *J Am Chem Soc*. 1975;*97*:1354–1358.

How to cite this article: Kraka E, Zou W, Tao Y. Decoding chemical information from vibrational spectroscopy data: Local vibrational mode theory. *WIREs Comput Mol Sci*. 2020;e1480. https://doi.org/10.1002/wcms.1480

APPENDIX A: PROGRAM PACKAGE LMODEA

The *local mode analysis* (LMODEA) program package shown in Figure A1 takes input information from a vibrational frequency calculation including (a) Cartesian coordinates, (b) Hessian matrix, (c) atomic masses, and (d) atomic polar tensors for intensities (if applicable). It contains interfaces for the most commonly used quantum chemistry packages, ensuring that LMODEA is generally available and does not depend on the use of a particular quantum chemical software. Important to note is that experimental frequencies can be provided for the analysis. The local mode parameters to be used can be defined in terms of internal coordinates including bond lengths, bond angles, and dihedral torsion angles, but LMODEA supports the use of curvilinear coordinates for local mode studies of intermediates during dynamic processes such as ring inversion, ring pseudo rotation and bond pseudo rotation in Jahn–Teller systems[319–322] and Cremer–Pople ring puckering and deformation coordinates[323] recently applied to the study of the interplay of ring puckering and hydrogen bonding in deoxyribonucleosides.[255] Other parameters include out-of-plane angles, pyramidalization angles, or parameters defined with regard to *dummy atoms* as needed for the description of strong and weak metal–π interactions. LMODEA will then produce local mode data and if requested perform a CNM analysis as shown in Figure 5. Python scripts interface the LMODEA output data to graphics software. It is important to note that the computational effort of an LMODEA analysis is comparable to that of a standard NBO analysis. The first beta-version of the code can be retrieved upon request.

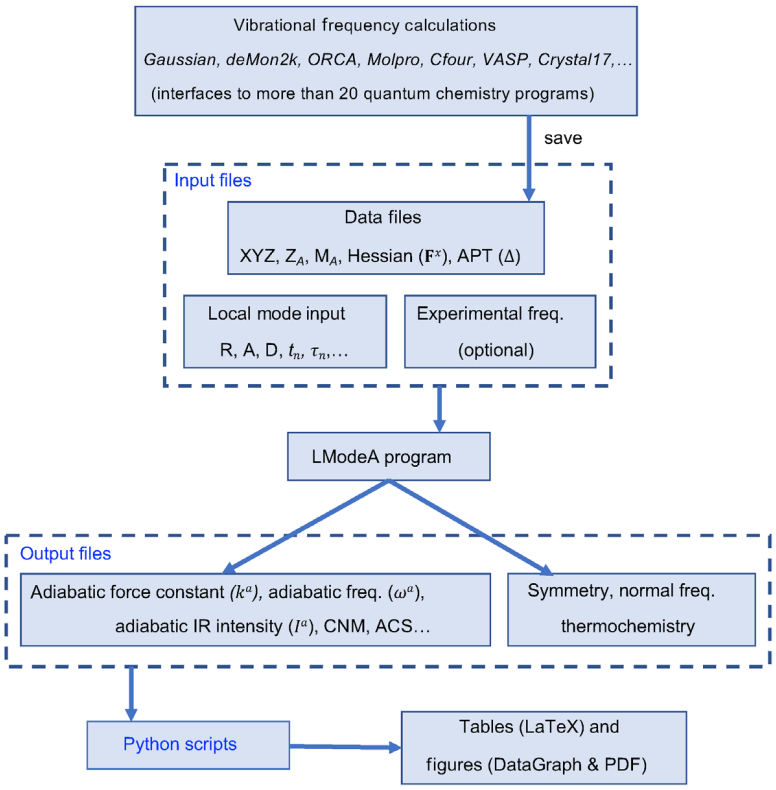

FIGURE A1 Flowchart of the local mode program LMODEA